The Silky Way: Biomimetic sensing through changes in structural proteins

Final report

Authors: Kenny Hey Tow[1], Desmond M. Chow[1], Fritz Vollrath[2], Isabelle Dicaire[3], Tom Gheysens[3] and Luc Thévenaz[1]

Affiliation:
[1] EPFL Swiss Federal Institute of Technology, Group for Fibre Optics, SCI-STI-LT, Station 11, CH-1015 Lausanne, Switzerland;
[2] University of Oxford, Department of Zoology, Oxford OX1 3PS, UK;
[3] Advanced Concepts Team, European Space Agency (ESA), Noordwijk, The Netherlands.

Date: 30 April 2015

ACT research category: Biomimetics

Contacts:

Kenny Hey Tow		Leopold Summerer (Technical Officer)	
Tel:	+41(0)216935604	Tel:	+31(0)715654192
Fax:	+41(0)216934660	Fax:	+31(0)715658018
e-mail:	kenny.heytow@epfl.ch	e-mail:	act@esa.int

Ariadna ID: 14-6401

Ariadna study type: Standard

Contract Number: 4000112060/14/NL/MV

http://www.esa.int/act

This page is intentionally left blank

ÉCOLE POLYTECHNIQUE
FÉDÉRALE DE LAUSANNE

Swiss Federal Institute of Technology (EPFL)
Group for Fibre Optics (GFO)
CH-1015 Lausanne
Switzerland

UNIVERSITY OF OXFORD

University of Oxford
Oxford Silk Group
Oxfordshire OX1 3PS
United Kingdom

FINAL REPORT FOR ARIADNA STUDY 14-6401

THE SILKY WAY: BIOMIMETIC SENSING THROUGH CHANGES IN STRUCTURAL PROTEINS

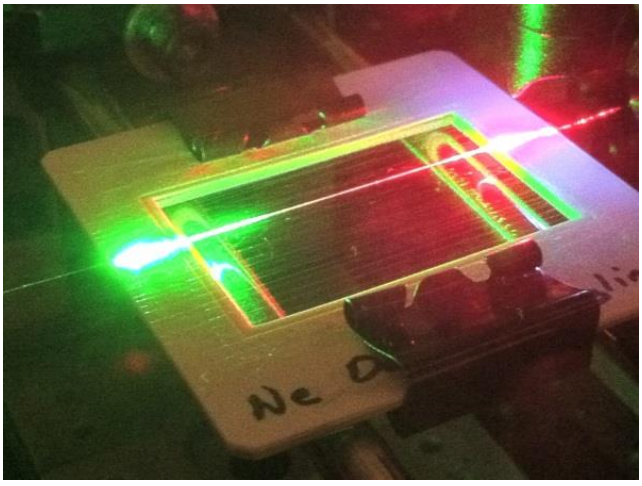

Light propagation along a sample of silk fibre

Illustration of a female *Nephila edulis* spider used by the Oxford Silk Group

Prepared by: **EPFL-GFO:** K. Hey Tow, D. M Chow and L. Thévenaz
Oxford Silk Group: F. Vollrath
ACT-ESTEC: T. Gheysens, I. Dicaire

This page is intentionally left blank

Ecole Polytechnique Fédérale de Lausanne (EPFL)
Group for Fibre Optics (GFO)
CH-1015 Lausanne, Switzerland

ABSTRACT

Whilst being thoroughly used in the textile industry and biomedical sector, silk has not yet been exploited for fibre optics-based sensing although silk fibres directly obtained from spiders can guide light and have shown early promises to being sensitive to some solvents.

The aim of Silky Way, which is to demonstrate the proof-of-concept of fibre optic biosensors based on a single strand of silk of the major ampullate gland, has been achieved during this six-month study.

First of all, light injection and guiding were achieved inside a spider silk dragline, controllably reeled from a female *Nephila edulis* spider. Indeed, efficient light injection inside these fibres allowed us to determine some optical characteristics of these silk fibres such as their transmission window, propagation losses and optical birefringence.

More specifically, the impact of biochemical agents on the properties of the transmitted light inside the silk fibre was assessed. We managed to demonstrate the use of spider silk dragline to detect polar solvents such as water, ammonia and acetic acid, which is a stepping stone to the development of fibre optic biosensors based on spider silk fibres.

Keywords: Biosensing, structural proteins, spider dragline silk, optical fibres, birefringence.

This page is intentionally left blank

Table of contents

List of Figures

List of Tables

1 INTRODUCTION

1.1 Scope of the document

This document is an end of activity report in the framework of the project "The Silky Way: Biomimetic Sensing Through Changes In Structural Proteins". This document is delivered according to the project study plan given in the EPFL/Oxford University technical proposal to answer CfP-14-6401 (4-6401), "The Silky Way: Biomimetic Sensing Through Changes In Structural Proteins" [AD1].

The content of this document reports all the research work, simulation and experimental activities accomplished at EPFL-GFO and Oxford Silk Group in the framework of Silky Way.

1.2 Plan of the document

This report is structured according to the following:

- Introduction, abbreviations and references
- Literature review of current optical biosensors and proposed concept for a new generation of biosensors based on spider silk
- Preparation of a silk optical fibre from a single major ampullate silk fibre (dragline) from a female spider of *Nephila edulis*
- Light injection inside a spider silk dragline
- Optical characterisation of the spider silk dragline
- Proof-of-concept of detection of biochemical agents with spider silk fibre

1.3 Applicable Documents

[AD1] ESA-ESTEC Invitation for proposal CfP 2014/1 (4-6401), "The Silky Way: Biomimetic Sensing Through Changes In Structural Proteins"

[AD2] EPFL/Oxford University technical proposal to answer CfP-14-6401 (4-6401), "The Silky Way: Biomimetic Sensing Through Changes In Structural Proteins", dated 14th of July 2014

1.4 Acronyms and Abbreviations

CfP	Call for Proposal
EM	ElectroMagnetic
EPFL	École Polytechnique Fédérale de Lausanne
ESA	European Space Agency
FOB	Fibre-Optic BioSensor
GFO	Group for Fibre Optics
MFD	Mode Field Diameter
MZI	Mach-Zehnder Interferometer
OTDR	Optical Time Domain Reflectometry
OSA	Optical Spectrum Analyser
RI	Refractive Index
TFOBS	Tapered Fibre-Optic BioSensor
WP	Work Package

1.5 List of References

[1] R. Narayanaswamy and O. S. Wolfbeis, *Optical sensors: industrial, environmental and diagnostic applications*. Springer Science & Business Media, 2004, vol. 1.

[2] B. Liedberg, I. Lundström, and E. Stenberg, "Principles of biosensing with an extended coupling matrix and surface plasmon resonance," *Sensors and Actuators B: Chemical*, vol. 11, no. 1, pp. 63–72, 1993.

[3] R. Heideman and P. Lambeck, "Remote opto-chemical sensing with extreme sensitivity: design, fabrication and performance of a pigtailed integrated optical phase-modulated mach–zehnder interferometer system," *Sensors and Actuators B: Chemical*, vol. 61, no. 1, pp. 100–127, 1999.

[4] B. H. Schneider, J. G. Edwards, and N. F. Hartman, "Hartman interferometer: versatile integrated optic sensor for label-free, real-time quantification of nucleic acids, proteins, and pathogens," *Clinical chemistry*, vol. 43, no. 9, pp. 1757–1763, 1997.

[5] N. J. Goddard, D. Pollard-Knight, and C. H. Maule, "Real-time biomolecular interaction analysis using the resonant mirror sensor," *Analyst*, vol. 119, no. 4, pp. 583–588, 1994.

[6] I. M. White and X. Fan, "On the performance quantification of resonant refractive index sensors," *Optics Express*, vol. 16, no. 2, pp. 1020–1028, 2008.

[7] J. D. Suter, I. M. White, H. Zhu, and X. Fan, "Thermal characterization of liquid core optical ring resonator sensors," *Applied optics*, vol. 46, no. 3, pp. 389–396, 2007.

[8] X. Fan, I. M. White, S. I. Shopova, H. Zhu, J. D. Suter, and Y. Sun, "Sensitive optical biosensors for unlabeled targets: A review," *analytica chimica acta*, vol. 620, no. 1, pp. 8–26, 2008.

[9] Y. Zhang, H. Shibru, K. L. Cooper, and A. Wang, "Miniature fiber-optic multicavity fabry-perot interferometric biosensor," *Optics letters*, vol. 30, no. 9, pp. 1021–1023, 2005.

[10] X. Wang, K. L. Cooper, A. Wang, J. Xu, Z. Wang, Y. Zhang, and Z. Tu, "Label-free dna sequence detection using oligonucleotide functionalized optical fiber," *Applied physics letters*, vol. 89, no. 16, p. 163901, 2006.

[11] K. Grattan and T. Sun, "Fiber optic sensor technology: an overview," *Sensors and Actuators A: Physical*, vol. 82, no. 1, pp. 40–61, 2000.

[12] G. Walsh, C. Sun, H. Xiao, N. Liu, J. Dong, and V. Romero, "An optical-fiber-based microsensor for explosives detection," pp. 62171L–62171L–6, 2006.

[13] S. Khalil, L. Bansal, and M. El-Sherif, "Intrinsic fiber optic chemical sensor for the detection of dimethyl methylphosphonate," *Optical Engineering*, vol. 43, no. 11, pp. 2683–2688, 2004.

[14] G. Schweizer, I. Latka, H. Lehmann, and R. Willsch, "Optical sensing of hydrocarbons in air or in water using uv absorption in the evanescent field of fibers," *Sensors and Actuators B: Chemical*, vol. 38, no. 1, pp. 150–153, 1997.

[15] H. S. MacKenzie and F. P. Payne, "Evanescent field amplification in a tapered single-mode optical fibre," *Electronics Letters*, vol. 26, no. 2, pp. 130–132, 1990.

[16] D. Littlejohn, D. Lucas, and L. Han, "Bent silica fiber evanescent absorption sensors for near-infrared spectroscopy," *Applied spectroscopy*, vol. 53, no. 7, pp. 845–849, 1999.

[17] M. Ahmad and L. L. Hench, "Effect of taper geometries and launch angle on evanescent wave penetration depth in optical fibers," *Biosensors and Bioelectronics*, vol. 20, no. 7, pp. 1312–1319, 2005.

[18] J. Villatoro, D. Luna-Moreno, and D. Monzón-Hernández, "Optical fiber hydrogen sensor for concentrations below the lower explosive limit," *Sensors and Actuators B: Chemical*, vol. 110, no. 1, pp. 23–27, 2005.

[19] S. Khijwania and B. Gupta, "Fiber optic evanescent field absorption sensor with high sensitivity and linear dynamic range," *Optics communications*, vol. 152, no. 4, pp. 259–262, 1998.

[20] L. Thévenaz, "Next generation of optical fibre sensors: new concepts and perspectives," vol. 9157, 2014, pp. 9157AN–9157AN–4.

[21] J. M. Matthews, *The textile fibres: their physical, microscopical and chemical properties*. J. Wiley & sons, 1913.

[22] C. I. Branden *et al.*, *Introduction to protein structure*. Garland Science, 1999.

[23] D. L. Kaplan, "Fibrous proteins: silk as a model system," *Polymer Degradation and Stability*, vol. 59, no. 1, pp. 25–32, 1998.

[24] C. Y. Hayashi and R. V. Lewis, "Molecular architecture and evolution of a modular spider silk protein gene," *Science*, vol. 287, no. 5457, pp. 1477–1479, 2000.

[25] K. Mita, S. Ichimura, and T. C. James, "Highly repetitive structure and its organization of the silk fibroin gene," *Journal of molecular evolution*, vol. 38, no. 6, pp. 583–592, 1994.

[26] Z. Shao and F. Vollrath, "The effect of solvents on the contraction and mechanical properties of spider silk," *Polymer*, vol. 40, no. 7, pp. 1799–1806, 1999.

[27] Z. Shao and F. Vollrath, "Materials: Surprising strength of silkworm silk," *Nature*, vol. 418, no. 6899, pp. 741–741, 2002.

[28] N. Huby, V. Vié, A. Renault, S. Beaufils, T. Lefèvre, F. Paquet-Mercier, M. Pézolet, and B. Bêche, "Native spider silk as a biological optical fiber," *Applied Physics Letters*, vol. 102, no. 12, p. 123702, 2013.

[29] K. Okamoto, *Fundamentals of optical waveguides*. Academic press, 2010.

[30] J. Von Der Weid, R. Passy, G. Mussi, and N. Gisin, "On the characterization of optical fiber network components with optical frequency domain reflectometry," *Journal of Lightwave Technology*, vol. 15, no. 7, pp. 1131–1141, 1997.

[31] M. Tachikura, "Internal loss measurement technique for optical devices equipped with fiber connectors at both ends," *Applied optics*, vol. 34, no. 34, pp. 8056–8057, 1995.

[32] R. Hui and M. O'Sullivan, *Fiber optic measurement techniques*. Academic Press, 2009.

[33] Y. Okamura, S. Yoshinaka, and S. Yamamoto, "Measuring mode propagation losses of integrated optical waveguides: a simple method," *Applied Optics*, vol. 22, no. 23, pp. 3892–3894, 1983.

[34] M. Monerie and P. Lamouler, "Birefringence measurement in twisted single-mode fibres," *Electronics Letters*, vol. 17, no. 7, pp. 252–253, 1981.

[35] S. Norman, D. Payne, M. Adams, and A. Smith, "Fabrication of single-mode fibres exhibiting extremely low polarisation birefringence," *Electronics Letters*, vol. 15, no. 11, pp. 309–311, 1979.

[36] A. Simon and R. Ulrich, "Evolution of polarization along a single-mode fiber," *Applied Physics Letters*, vol. 31, no. 8, pp. 517–520, 1977.

[37] K. Kikuchi and T. Okoshi, "Wavelength-sweeping technique for measuring the beat length of linearly birefringent optical fibers," *Optics letters*, vol. 8, no. 2, pp. 122–123, 1983.

[38] D. J. Little and D. M. Kane, "Image contrast immersion method for measuring refractive index applied to spider silks," *Opt. Express*, vol. 19, no. 20, pp. 19182–19189, 2011.

[39] F. S. Parker, *Applications of infrared, Raman, and resonance Raman spectroscopy in biochemistry*. Springer Science & Business Media, 1983.

[40] Z. Shao, F. Vollrath, J. Sirichaisit, and R. Young, "Analysis of spider silk in native and supercontracted states using raman spectroscopy," *Polymer*, vol. 40, no. 10, pp. 2493–2500, 1999.

[41] D. Goldstein and D. H. Goldstein, *Polarized Light, revised and expanded*. CRC Press, 2011, vol. 83.

[42] C.R. Webster, P.R. Mahaffy, S.K. Atreya, G.J. Flesch, M.A. Mischna, P.Y. Meslin, ... & M.T. Lemmon, "Mars methane detection and variability at Gale crater," *Science*, 347 (6220), 415-417, 2015.

[43] F.J Martín-Torres, M.P. Zorzano, P. Valentín-Serrano, A.M. Harri, M. Genzer O. Kemppinen, & D. Vaniman "Transient liquid water and water activity at Gale crater on Mars," *Nature Geoscience*, 2015.

2 TOWARDS A NEW GENERATION OF FIBRE-OPTIC BIOSENSOR

The goal of this study is to demonstrate the proof-of-concept of fibre optic biosensors based on spider dragline silk. Positive results could bring a major breakthrough in the optical fibre biosensing field. Firstly, the use of a sensing fibre made from a chemically sensitized material such as silk will considerably simplify the interrogation and detection sensing system since we will no longer require complex setups based on evanescent-field sensing. Secondly, this will pave the way for the fabrication of a new generation of economical and custom-made FOBs since spider silk can be spun at ambient conditions. Moreover, silks can be functionalized to be even more sensitive to any type of biochemical or particular environmental quantities by incorporating specific dyes making them very cost-effective for potential artificial industrial production of silk-based fibres with unique properties.

2.1 Literature review on current biosensors

Biosensors are nowadays extensively used for many industrial, environmental and diagnostic applications including biomedical research, health-care, pharmaceuticals, environmental monitoring, homeland security, and the battlefield [1].

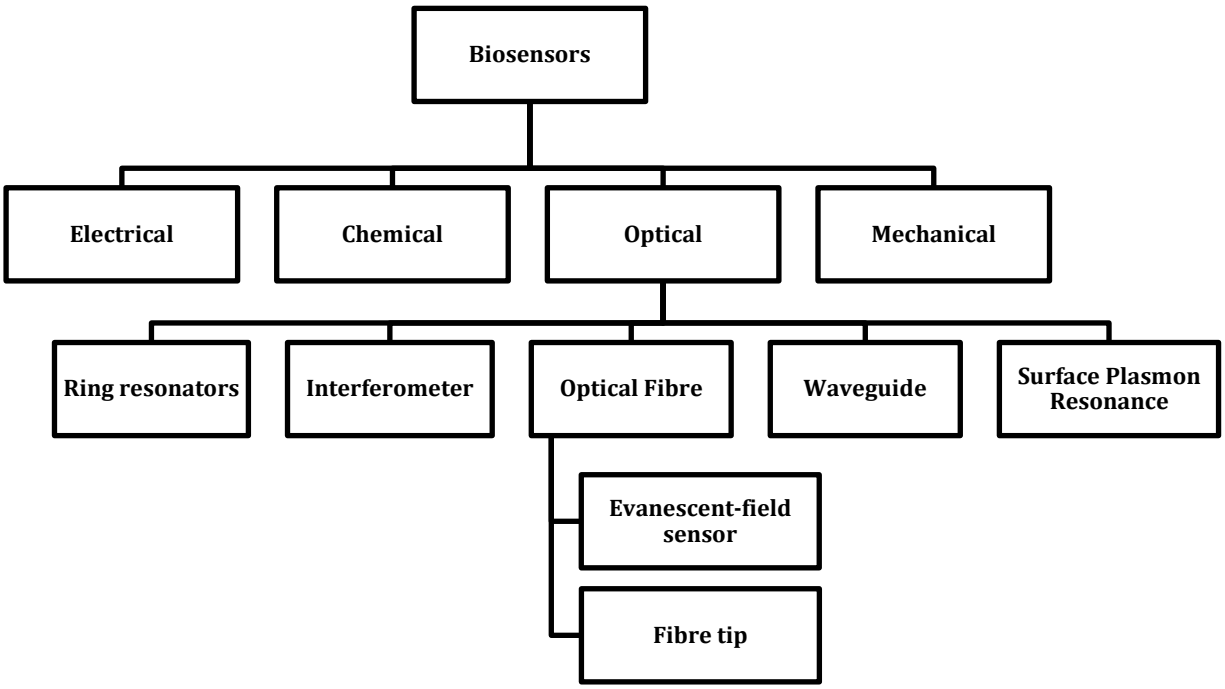

Figure 1: Classification of existing biosensors based on type of biotransducer (1st level), on the technological platform used (2nd level) and on the method used (3rd level).

They can be classified (Figure 1) according to the type of biotransducer they employ:

- Electrical
- Chemical
- Mechanical
- Optical

In the past few years, optical sensors have been under intensive research and deployment as biological and chemical sensors. For these applications, small size, high sensitivity, high selectivity and low detection limits are the dominant requirements. Conventional optical biosensors are based on these technologies:

- Surface plasmon resonance [2]
- Interferometer [3, 4]
- Optical waveguides [5]
- Ring resonator [6, 7]

They exhibit typical detection limits (*DL*) for bulk solution sensing in the range of 10^{-4} - 10^{-7} in refractive index (RI) units [8]. DL is defined as:

$$DL = \frac{\sigma}{S}, \qquad \textbf{(1)}$$

where S is the sensitivity and σ is the noise level.

These devices can reach *DL* levels in the range of μg-ng ml^{-1} for biomarkers in medical diagnostics applications and micromolar to nanomolar concentrations for protein detection [8]. However, most of these systems cannot discriminate between various analytes and are less sensitive to large molecules. In addition, low detection limits can only be achieved via incremental steps such as improving the detection system (to lower the noise level) or modifying the optical structure e.g. via chemical etching, gold nanoparticles, nanoscopic fibres, structural slow light or nanoscopic slots to enhance the sensitivity.

2.2 Fibre-Optic Biosensors (FOBs)

Fibre-optic biosensors (FOBs) are optical fibre-based devices used to measure biological molecular species such as proteins, nucleic acids, etc. [9, 10] and are promising alternatives to conventional biosensors because they encompass all the advantages linked to the use of optical fibres:

- Low cost
- Small size
- Compatibility to a wide range of surface modifications
- Potentiality for remote sensing
- Availability of inexpensive lasers and photodetectors

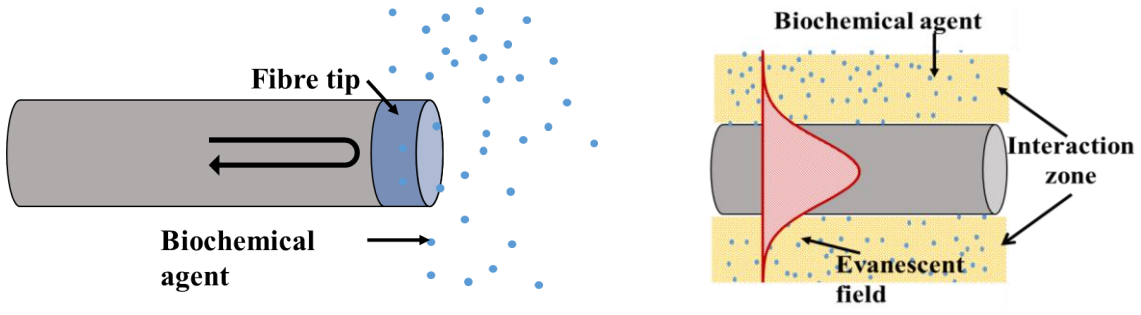

(a) (b)

Figure 2: Typical fibre-optic biosensors based on (a) fibre tip and (b) evanescent field sensing.

The working principle of FOBs requires direct interaction between light and the substance to be detected. Generally, the optical fibre is solely used as convenient photon transport vectors [11]. For FOBs using sensitive fibre tips (Figure 2(a)), they are only used to transport light from the optical source to and from the sensing region in order to detect the adsorption-induced change of the reflectivity brought by the presence of the biochemical. For instance, a MFI zeolite film can be grown on the end surface of an optical fibre [12] for TNT vapour detection.

Another way to create light-gas interaction in the fibre's surrounding is to force the light confined inside the optical fibre to partially or totally propagate out of the fibre (Figure 2(b)). Hence, the sensitivity of these sensors depends on the Φ, the fraction of the optical power present in the evanescent field as compared to the total optical power.

Classical optical fibres used for telecommunications being mainly intended for light propagation with minimal loss, the evanescent field is entirely contained within the cladding thus not allowing light interaction with species surrounding the fibre. Even if the cladding is removed, Φ remains too small for sensing applications, as a result of the high RI contrast. Several techniques, summarized in

Table 1, can be used to enhance the evanescent field and facilitate mode coupling for increased sensitivity. For instance, the passive cladding of an optical fibre can be replaced over a small section by a chemical dye sensitive to dimethyl methylphosphonate so that any change in the optical or structural characteristic of the chemical dye due to the presence of the species vapours, will cause an effective index and absorption change in the fibre, changing its transmission properties [13].

Table 1: Different methods currently used to increase the interaction between the light evanescent field and the biochemical species.

Method	Basic principle	Ref.
Sensitive material	Passive cladding is replaced by a sensitive material	[13]
Sensitive cladding	Cladding is specially designed to be sensitive to species to be detected	[14]
Fibre tapering	Core/clad is reduced to increase the evanescent field magnitude and penetration depth.	[15]
Fibre bending	Bending results in light loss and increase in evanescent field	[16]
Launch angle	In multimode fibres, light can be launched at different angles (several modes).	[17]
Working wavelength	Penetration depth increases with wavelength	[18]

Tapered fibre-optic biosensors (TFOBS) [19] are also commonly used. A tapered fibre is obtained by drastically reducing the optical fibre size from 125 μm to values typically in the order of one micron. Fibre tapering not only exposes the evanescent field to the surroundings by forcing part of the EM field to propagate outside the fibre, but also increases the overlap percentage Φ, thereby increasing the sensing capacities. However, all these solutions rely on the evanescent part of the EM field for detection and are therefore limited in their effect since they use only a small fraction of the total field for interaction. If one aspires for a more extended evanescent field, tapered fibres with sub-micron diameters must be used, bringing these drawbacks:

- Sub-micron tapers with waist lengths of the order of a few mms are very difficult to be fabricated and handled.
- They do not have a long lifetime since their losses can increase up to 20-30 dB due to exposure to environmental factors such as humidity, dust particles, etc.

2.3 A new, simplified architecture for biochemical detection

A more disruptive approach would be to directly use the optical fibre itself as the sensing element. The biochemical agents would then directly modify the properties of the fibre material in its entire volume; thereby changing the properties of light propagating inside the fibre.

The general principle of such a sensor is outlined on Figure 3: light from an optical source is injected inside the sensing fibre, the agent will interact with the fibre material and any induced change in the fibre's properties due to the presence of the agent will subtly alter the parameters of the transmitted light (intensity, wavelength, phase, spectrum, polarisation) in the fibre, which can be analysed and interpreted. Subsequently, the architecture of the sensing system is considerably simplified, since no evanescent-field coupling is required and the entire optical field interacts with the chemically sensitized material, therefore it is less energy-consuming compared to current optical fibre biosensors. Moreover, a transmission setup excludes the risk of any contamination by other unwanted agents or dust since light is strictly kept confined inside the fibre.

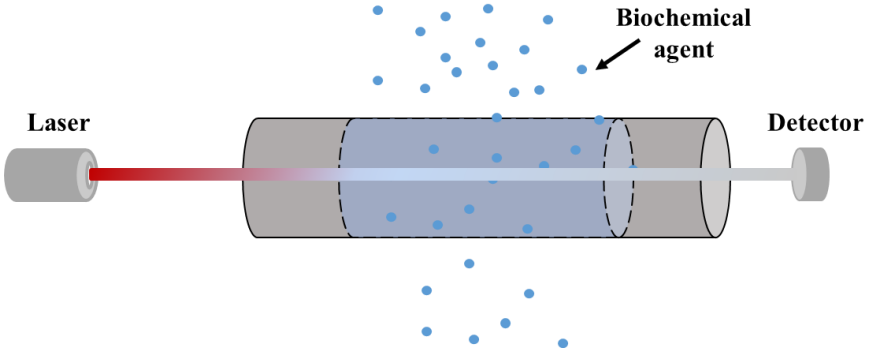

Figure 3: Proposed simplified interrogation technique for our novel biosensor based on silk fibre. The presence of the biochemical agent modifies the material properties of the fibre, which can be quantified by analysing the properties of light transmitted along the fibre.

Silica optical fibres are commonly used for sensing physical parameters such as temperature, mechanical strain, vibrations, pressure acceleration, rotations (gyroscopes) but they are very poorly or even not at all sensitive to chemical or biological compounds [20]. Considering the high solidification temperature of silica, complex reactive molecules cannot be incorporated in the silica material while keeping their chemical integrity.

2.4 Why use silk fibres?

Hence, the underlying idea here is to choose an optical fibre made of a material whose mechanical and optical properties would be potentially altered in the presence of biochemical agents, paving the way for the use of a reactive fibre, which is capable of interacting with its environment. Horse hair has long been known to expand with increasing humidity forming the basis of old hygrometers. Also, natural industrially available fibres like cotton, flax and wool are sensitive to humidity. However, these fibres contain a lot of impurities, like waxes, fatty acids, polyphenols, sugars, etc., and are generally cross-linked, thus making them less sensitive for sensing environmental compounds. In contrast, the industrially obtained silk from the silk moth *Bombyx mori* is a good candidate, but like

the aforementioned fibres, it has an irregular cross-section (triangular), making them less suitable for light coupling.

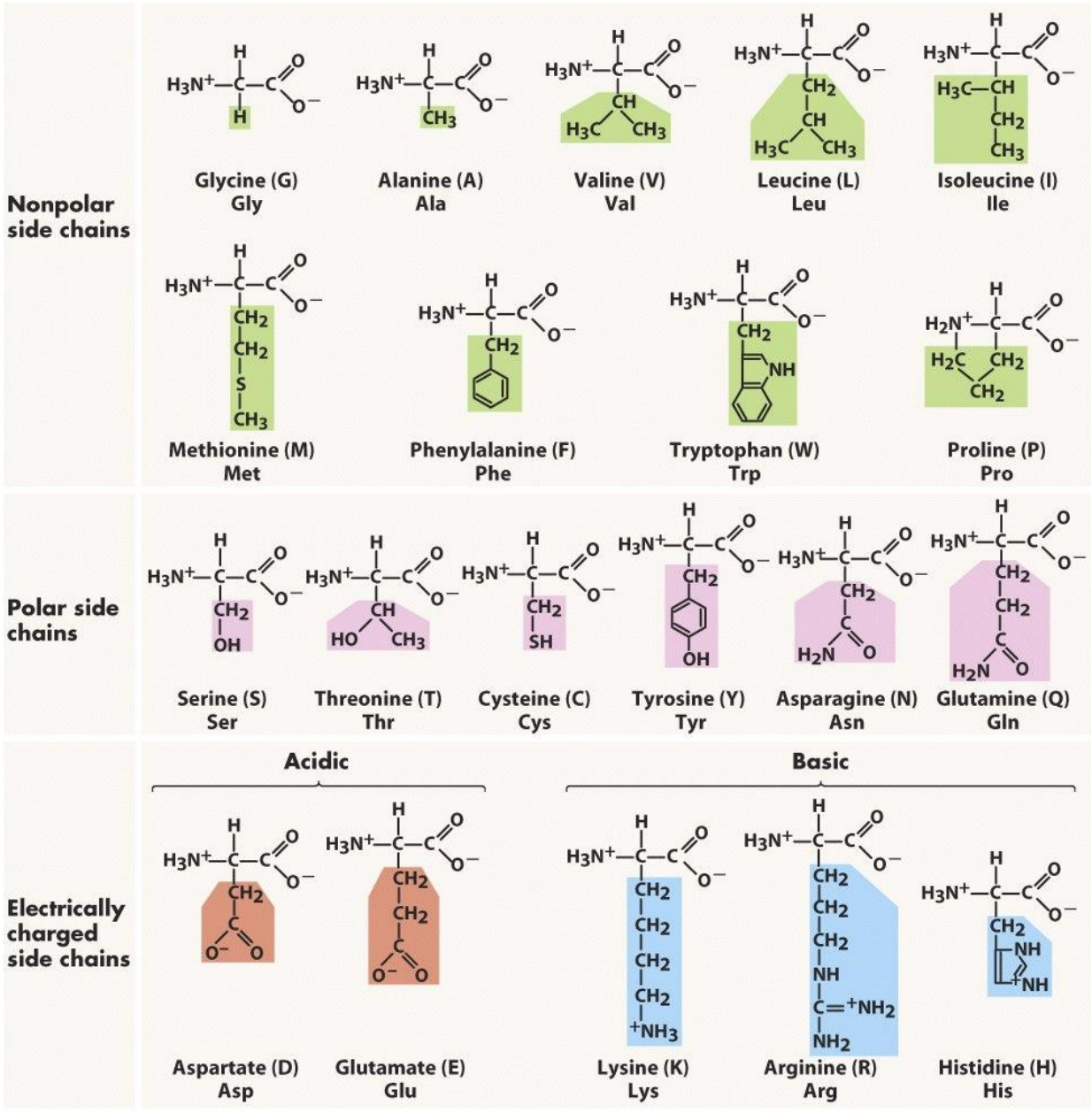

Figure 4: The twenty amino acids in nature grouped according to polarity and electrical charge (© 2005 Pearson Prentice hall, Inc.)

Spider silk, however, forms the perfect candidate as it does not have any of the aforementioned shortcomings and possesses all necessary characteristics for a perfect multi-purpose biosensor. Their beneficial properties are listed in more detail below:

1. Ability to guide light

Spider silk filaments have long been used in the optical industry as cross lines in various instruments in astronomy and surveying, such as telescopes and microscopes [21]. Very recently,

light guiding in spider dragline silk of *Nephila clavipes* has been demonstrated in the region of 800 nm by direct coupling [28], thereby paving the way towards the use of spider silk fibres for optical sensing.

2. Composition

Silks are protein threads composed of repeating arrays of polypeptides that contain both discrete crystalline and non-crystalline domains that are oriented around a fibre axis. The molecular backbone of all proteins consists of a chain of amino acids that are linked by peptide bonds to form a polypeptide chain.

There are 20 different amino acids (Figure 4) that can make up proteins but the order and abundance of the amino acids composing a protein is defined by the genetic code (DNA). The amino acids are usually divided into three different classes defined by the chemical nature of the side chain:

- The first class comprises those with strictly *hydrophobic side chains*: alanine (Ala (A)), valine (Val (V)), leucine (Leu (L)), isoleucine (Ile (I)), phenylalanine (Phe (F)), proline (Pro (P)) and methionine (Met (M)) (Figure 4).
- The second class comprises of four *charged residues* namely aspartic acid (Asp (D)), glutamic acid (Glu (E)), lysine (Lys (K)) and arginine (Arg (R)) (Figure 4).
- The third class comprises those with *polar side chains*: serine (Ser (S)), threonine (Thr (T)), cysteine (Cys (C)), asparagine (Asn (N)), glutamine (Gln (Q)), histidine (His (H)), tyrosine (Tyr (Y)) and tryptophan (Trp (W)) (Figure 4).

  The amino acid glycine (Gly (G)), which has only a hydrogen atom as a side chain and is therefore the simplest of the 20 amino acids, has *special properties* and is usually considered either to form a fourth class or to belong to the first class [22].

Table 2. Types and functions of spider silk for *Araneus diadematus* [23].

Silk	Gland	Amino acids[a]
Dragline	Major ampullate	Gly (37%), Ala (18%), small side safety line chains (62%), polar (26%)
Viscid	Flagelliform	Gly (44%), Pro (21%), small side chains (56%), polar (17%)
Glue-like	Aggregate	Gly (14%), Pro (11%), polar glue (49%), small side chains (27%)
Minor	Minor ampullate	Gly (43%), Ala (37%), small side chains (85%), polar (26%)
Egg sac	Cylindrical (tubuliform)	Ser (28%), Ala (24%), small side chains (61%), polar (50%)
Wrapping	Aciniform	Ser (15%), Gly (13%), Ala (11%), small side chains (40%), polar (47%)
Attachment	Piriform	Ser (15%), small side chains (32%), polar (58%)

This amino acid composition of the same type of silk will vary intra and interspecific, and one spider can have up to 7 different silk types all with their own specific amino acid composition (Table 2). The silk of interest here is the dragline silk or major ampullate silk, secreted by the major ampullate glands and is composed mainly of glycine (30-40%) and alanine (20-30%). Also

the amount of glutamine (Glu) exceeds 10%, while the amount of proline seems to vary depending on the spider species between 5 and 15%.

This indicates that the fibre is partly hydrophobic and partly hydrophilic meaning that entering chemical compounds with different behaviours, like different hydrophobicity, will bind to different and specific amino acids in the fibre.

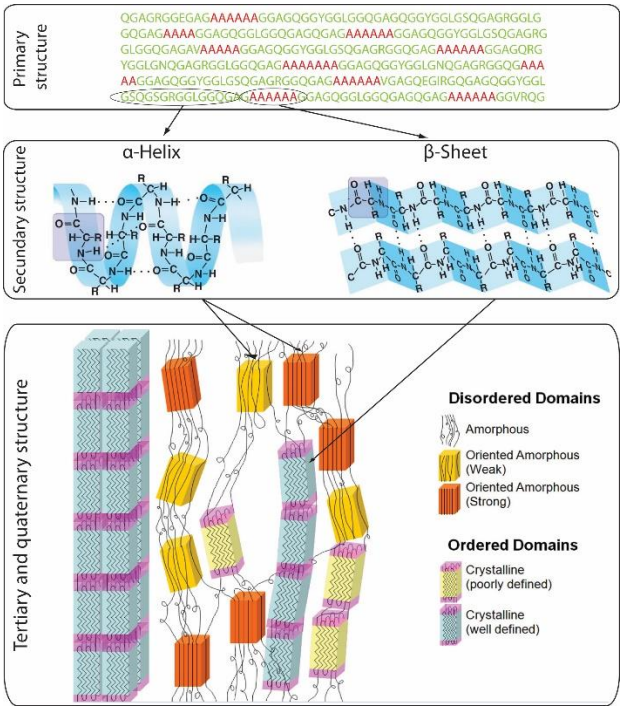

Figure 5: Organization of amino acids in a primary sequence resulting into a secondary structure and ultimately in a tertiary and quaternary structure. (adjusted from ©2008 Pearson Education, Inc., publishing as Pearson Benjamin Cummings)

These amino acids will be organized in a sequence determined by the DNA which is named the primary structure (Figure 5), or in other words, the arrangement of the amino acids along the linear polypeptide chain [22]. Different regions of the sequence form local regular secondary structures, such as α-helices or β-sheets (Figure 5). The formation of secondary structure in a local region of the polypeptide chain is to some extent determined by the primary structure. Certain amino acids favour either α-helices or β-sheets; others favour formation of loop regions. A unique structural feature shared by silk protein sequences is their organisation into two types of alternating blocks or domains (Figure 5). One is composed of small repetitive units, forming the β-sheet type of block, which tends to be hydrophobic and forms the crystalline blocks [24, 25]. The other type of block is non-repetitive and tends to be the most hydrophilic part of the core sequence making up the amorphous regions. This sequence is short compared to the size of the more hydrophobic repetitive block and is referred to as a "spacer". This secondary structure then organizes further into a tertiary and quaternary structure making up the nano-fibrils, organising even further into micro-fibrils into the ultimate silk fibres.

As hydrophobic and hydrophilic amino acids are grouped together in the fibre forming defined α-helical and β-sheet domains, chemicals with defined properties will have very defined and specific interactions with these domains. Interacting molecules with these regions can either bind to the α-helical portion thereby affecting the elongation properties of the fibre or the orientation of the crystalline β-sheet blocks. In contrast molecules interacting with the β-sheet blocks will either

change the crystallinity of the fibre or the orientation of the crystalline blocks in such a way that the modulus and breaking stress of the fibre are changed. All these changes are also expected to change the light propagation into the fibre and therefore a multitude of compounds can be detected with only a single silk fibre as many different interaction modes are possible.

As discussed before, many different types of silk exist and many more different spider species resulting in an unlimited supply of different fibres with their very specific primary amino acid composition and therefore also their own very specific interactions with chemical compounds. This also means that some silks will be more suited than others for sensing of specific chemical species and that also the sensitivity will be dependent on spider silk type.

3. Morphology

Another advantage of spider silk is that the amount of crystalline and amorphous regions in the fibre can be consistently tuned in a very cost-effective way, as it is spun at ambient conditions. The selection of the type of silk and the spinning of the silk fibre can be controlled by forcible reeling of the selected type of silk of the spider. By changing the reeling speed and environmental conditions, silk can be obtained with a known amount of crystalline and amorphous regions required for sensing.

Moreover, in contrast to previously discussed natural fibres, spider silk fibres have all essential properties for the optical coupling of light into fibres, like a smooth surface, a circular fibre cross section and no additives (like wax, fat, etc.) in the silk fibre besides proteins.

4. Sensitivity

Unlike most natural fibres, spider silk fibres are held together by reversible hydrogen bonding, which can be changed by polar and non-polar solvents making them ideal for detecting modifying agents such as water molecules, acids, bases, etc. Earlier research has shown that spider silk super-contracts in water as well as in a range of polar solvents such as methanol, ethanol and urea solutions [26].

The proteins making up silk fibres are very large (330kDa) in contrast to other known proteins. One such protein consist of several hydrophobic (mainly β-sheet blocks) and hydrophilic regions (mainly α-helical portions) and therefore would be able to bind several molecules. As the silk fibre is composed of many billions of these proteins implies that one silk fibre will be able to bind many molecules and thus the signal-to-noise ratio would be very high, resulting in a highly sensitive sensor.

In this study, a single strand of silk of the major ampullate gland controllably reeled from *Nephila edulis* was used as a model for the following reasons:

- *Nephila edulis* is one of the best studied species and best documented in the literature.
- This spider species produces one of the thickest silk fibres of all spiders, thereby facilitating easier handling. Moreover, the thicker the fibre the easier the light coupling.
- This silk can be easily manually selected with the help of some tweezers and binoculars, and can be reeled under controlled conditions like reeling speed, humidity and temperature.
- This species is bred in-house at the Oxford Silk Group (Oxford University) and is continuously available due to the fact that their life-cycle is uncoupled from seasonal cycles.

3 FROM SPIDER DRAGLINE TO SILK OPTICAL FIBRE

3.1 Spider reeling, fibre sample preparation and property testing

A single major ampullate silk fibre (dragline) from a female spider of *Nephila edulis* was reeled onto two spools. One spool was reeled at 5 mm/second (Labelled A) and the other spool was reeled at 37 mm/second (Labelled B). The silk on both spools was reeled from the same spider and same spigot, and the silk on spool A was reeled before that of spool B. The reason for reeling two different samples was to obtain two different fibre types namely one thinner and more crystalline fibre obtained by reeling at a high speed and a second fibre type that is thicker and more amorphous (less crystalline) reeled at slower speed. Both properties have an advantage in optics as it is easier to couple light in thicker fibres and more crystalline fibres, however in spider silk it is difficult to combine these two properties in a single fibre.

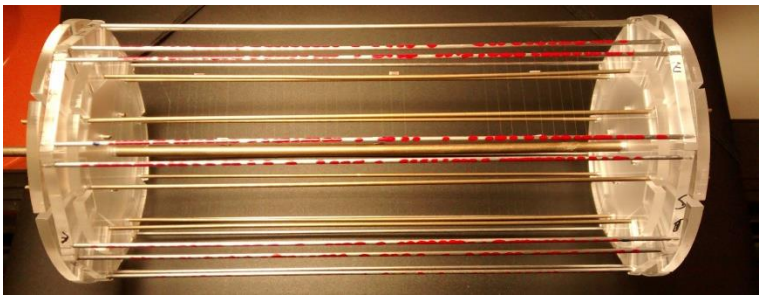

(a)

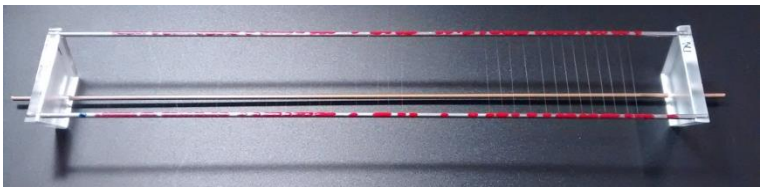

(b)

Figure 6: a) One reeling spool on which the silk is reeled of which we had two, A and B. b) Sector of a reeling spool with the tensioned reeled fibres.

From each spool three fibre samples were tested, for their tensile properties and diameter at the following positions on the reel; one at the beginning (Segment 3-1), one in the middle (Segment 3-2) and one at the end of the reel (Segment 3-3). Three tensile and diameter measurements[1] were made for each spool, A and B, to investigate the changes in fibre properties during reeling and to check the consistency of the reeling process. The positions from where the samples have been marked on the reels; Z1, Z2 & Z3 for tensile measurements and S1, S2 & S3 for diameter measurements.

In contrast to what was expected, we found that the fibre diameters were quite similar between the two spools despite the different reeling speeds that were used. The diameter of the fibre was a little higher

[1] **Diameter Measurements:** All samples were investigated using a Jeol JCM 5000 Neoscope (Benchtop SEM). A total of 10 diameter measurements were made for each sample at a magnification of 2700x and the average value was calculated to result in the final diameters. **Tensile Measurements:** All samples were investigated using a Zwick/Roell Z0.5 single column Universal Testing Machine configured in tensile testing mode. Samples were mounted on a standard 15 mm length card frame for handling and loading. Once mounted the sides of the card frame were cut so that only the fibre was connecting the two clamps. The instrument then extended the sample at a rate of 30%/minute until it broke.

at lower reeling speeds, namely 5.6µm, then at higher reeling speeds, namely 5.0µm, but only differed by 0.6µm. This difference is somewhat smaller than expected, namely 1 to 1.5µm, and therefore the difference between both spools is very small.

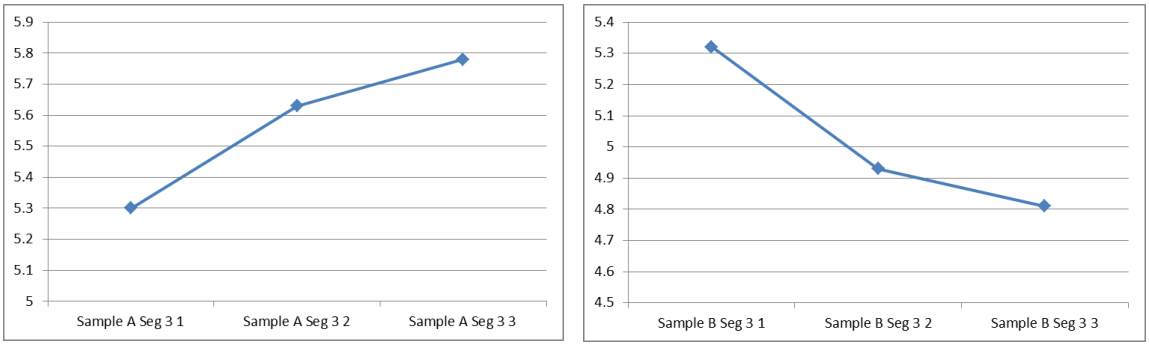

Figure 7: Both graphs show the diameter change in the spool during reeling from the beginning (1), via the middle (2) to the end (3) in spool A and spool B reeled at respectively 5 and 37mm/s.

Within the fibres of spool A the fibres tend to increase in diameter from the beginning of the spool till the end with a maximum increase of about 0.5um. In contrast, the fibres of spool B tend to decrease in diameter from the beginning of the spool till the end with a maximum decrease of about 0.5um. Again this difference in diameter is very low and thus negligible as the measuring error is in the same range.

Table 3: Below, the tensile properties are tabulated indicating the breaking stress (Fmax), initial modulus (Emod), strain (%) and the diameter (µm), with the average per spool A (green) and B (orange).

Sample name	Strain %	E_{mod} Mpa	F_{max} N	F_{max} MPa	Diameter µm
Sample A Seg 3 1	33.81243	9555.53321	0.023206	1052.40	5.3
Sample A Seg 3 2	34.21935	8355.22461	0.02824	1134.96	5.63
Sample A Seg 3 3	34.59353	8731.30129	0.027063	1031.93	5.78
	34.2	**8880.7**	**0.026**	**1073.1**	**5.6**
Sample B Seg 3 1	19.46477	11738.3455	0.030854	1388.72	5.32
Sample B Seg 3 2	20.97928	12131.8476	0.026702	1399.52	4.93
Sample B Seg 3 3	19.13311	12491.415	0.024003	1321.63	4.81
	19.9	**12120.5**	**0.027**	**1370.0**	**5.0**

Comparing the tensile properties of both spools A and B reeled at different speeds resulted in quite different stress-strain graphs. This change in tensile properties was expected as higher reeling speeds results in stiffer silk fibres [27]. This is also what is seen in our data, comparing the reeling speed at 5mm/s and 37mm/s a decrease was seen in the strain from 34.2 to 19.9%, whereas the modulus and breaking stress increased by 36.5%, from 8880.7 to 12120.5MPa, and 27.6%, from 1073.1 to 1370.0MPa respectively. So reeling at low speed results in less crystalline fibres with thicker diameters and are therefore more elastic. In contrast, reeling at higher speed results in more crystalline fibres, thus less amorphous regions, with a thinner diameter and therefore are stronger and less elastic.

When considering the data from the spools individually, it can be concluded that the mechanical properties are identical and therefore also the crystallinity and composition of the fibre. This means

that the fibre has identical properties and therefore should exhibit consistent light propagation and sensing properties.

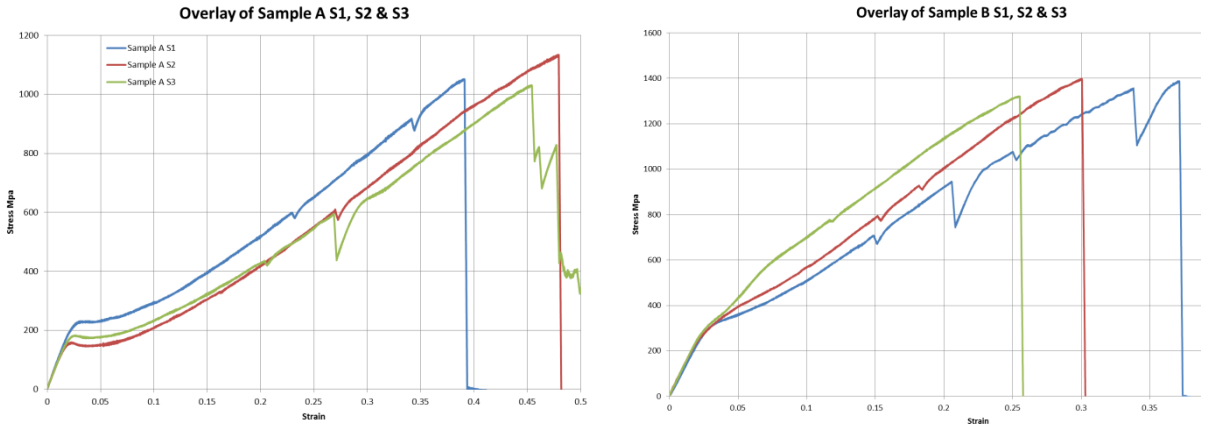

Figure 8: Stress-strain graph of the three fibres of the two spools A and B showing very little variation.

To summarize, a single major ampullate silk fibre from a female *Nephila edulis* spider was reeled onto a spool by the Oxford Silk Group. The reeling process under controlled speed resulted in very uniformly spun fibres with a smooth surface, equal circular diameters and identical material properties, which is of vital importance for its optical properties. This means that fibres tested form the same spool should all consistently exhibit the same structural changes after interacting with chemical agents. For further experimental testing, fibres of spool A were used that were reeled at 5mm/s as these were a little thicker and therefore somewhat easier to work with. The fibre samples that were used had a diameter of 5.6 µm.

3.2 Silk dragline as optical fibre

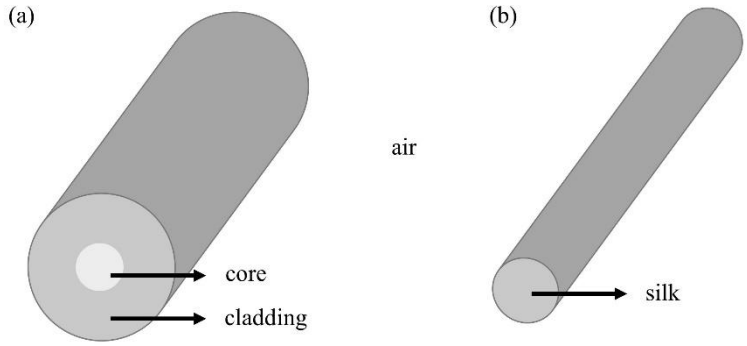

Figure 9: Structure of (a) standard optical fibre (b) silk fibre

The conventional optical fibre is comprised of a transparent core surrounded by a transparent cladding material with a lower RI (Figure 9). Light is guided in the core by total internal reflection. As dragline silk is transparent in the vicinity of visible wavelength region and has a RI of ~1.5, light can be guided inside as in typical optical fibre when it is surrounded by a medium with lower RI (i.e. air n=1, water n=1.333), as shown in Figure 9. However, due to the absence of a thick cladding layer with RI near to that of the core, the RI contrast between silk and its surrounding (air) is high, resulting in multimode guidance. The number of guided modes in an optical fibre is determined by V number, which is proportional to the core-cladding RI difference and core diameter but inversely proportional to the wavelength of light. V number must be less than 2.405 for single mode guidance. In the case where the

dragline silk is surrounded by air, it is estimated to be ~28 at 635 nm. The comparison between a standard telecom fibre (SMF-28) and silk fibre is shown in Table 4.

Table 4: Comparison between a standard telecom fibre (SMF-28) and silk fibre

Parameters	Silk fibre	SMF-28
Fibre diameter	~5 µm	125 µm
Core diameter	-	~8 µm
Operating band	600-1350 nm	1310-1650 nm
Single-mode guidance	No	Yes
RI	~1.54 (635 nm)	~1.44 (1550 nm)
RI contrast	~0.54	~0.005
Attenuation	~10 dB/cm	0.2 dB/km
Coating	-	Acrylate

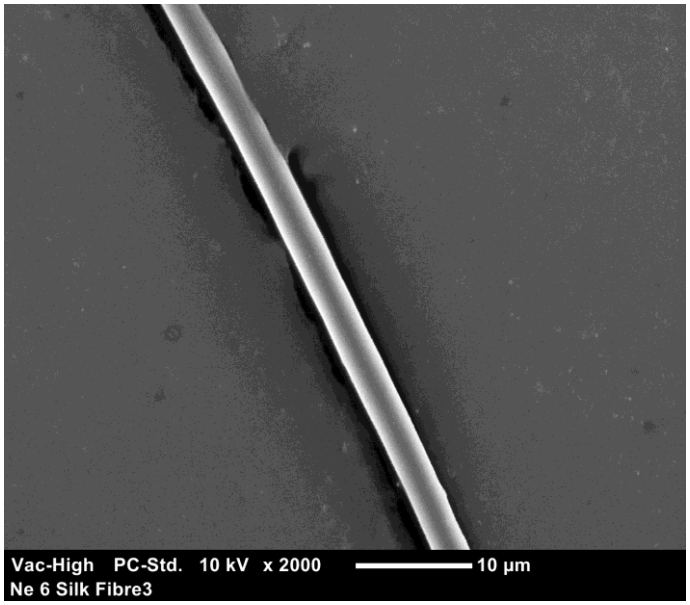

Figure 10: Scanning electron microscope *(*SEM*)* image of a collected silk dragline

The scanning electron microscope (SEM) image of a silk fibre sample, with a diameter of 5.6 μm, used for light injection is shown on Figure 10. The reeling process under controlled speed resulted in a very uniformly spun fibre with a smooth surface, equal circular diameters and identical material properties, which is of vital importance for its optical properties.

4 LIGHT INJECTION INSIDE THE SILK FIBRE

Light injection into the dragline silk is the most crucial part of this exploratory work as it determines the success of the ensuing optical properties characterisation and sensing demonstration. In fact, light guiding in spider silk has been reported before in [28]. In this Ariadna study, we worked on two coupling techniques that are robust and repeatable: evanescent field coupling and direct light injection. Each method has its own share of pros and cons; therefore the method selection depends on careful judgement based on the requirements and objectives of each study.

Evanescent field coupling is realised by launching light into a half-tapered fibre with the tapered end near to that of the dragline silk. As both the tapered fibre and silk are placed close to each other, power exchanges alternatingly between the tapered fibre and silk along the parallel length through evanescent field. This method is non-invasive and more suitable for studying dragline silk in its pristine condition. However, the efficiency of evanescent field coupling depends largely on light wavelength, polarisation, RI of silk, diameter of silk and separation between silk and tapered fibre. This efficiency can even reach 100% if the two coupled waves propagate at the exact same velocity. The limited bandwidth of evanescent field coupling method also prevents the study of spectral transmission.

Direct coupling method is achieved by launching light directly into the silk fibre from one of the two ends. We used two techniques for direct coupling: 1) launching light from a bent section of silk fibre and 2) through end facet of immobilised silk fibre. The following section describes the coupling methods in detail.

4.1 Evanescent field coupling

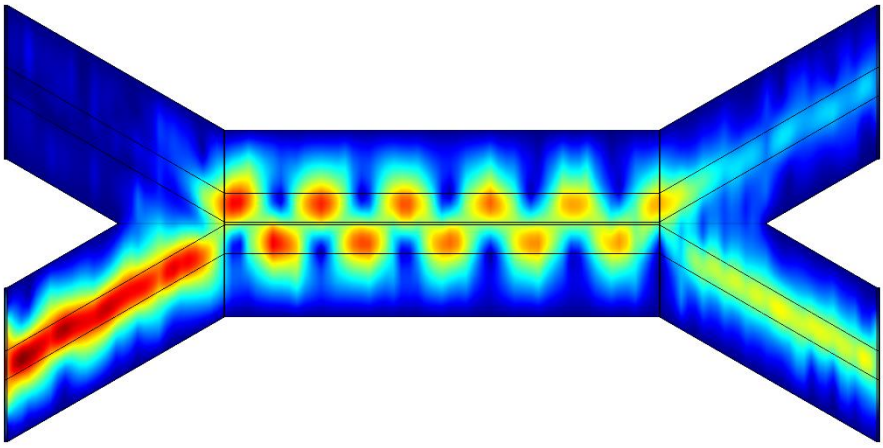

Figure 11: Optical coupling between two co-propagating waveguides.

The principle of evanescent field coupling is based on coupled-mode theory. As two waveguides are in close proximity with each other, they are optically coupled and exchange power periodically along the parallel co-propagating length, illustrated in Figure 11. The power coupling efficiency depends on a few factors, namely the separation between waveguides, RI of waveguides, length and size of each waveguide. Details on coupled-mode theory are described in [29]. Power coupling between two co-propagating waveguides is a sinusoidal square function along the coupling length and the maximum efficiency depends on electric field overlapping and propagation constant difference of both waveguides. In order to optimise the coupling, overlapping of electric field should be maximised whereas the effective RI difference of the two fibres should be minimised. Due to the large difference of RI between the silk fibre and silica tapered fibre, coupling of fundamental modes between the two fibres is not possible considering the required size of silk fibre for such coupling to happen is ~0.7 µm for tapered fibre of ~5 µm, as indicated in Figure 12. As a result, evanescent field coupling occurs between higher-order modes from both fibres. Since there is a multitude of possible higher-order

guided modes in both fibres, as shown in Figure 13, a detailed quantitative analysis of actual coupling condition would be laborious. A more practical approach in addressing the coupling efficiency is through fine adjustment through experiments based on qualitative parameters, which are the electric field overlapping and coupling length.

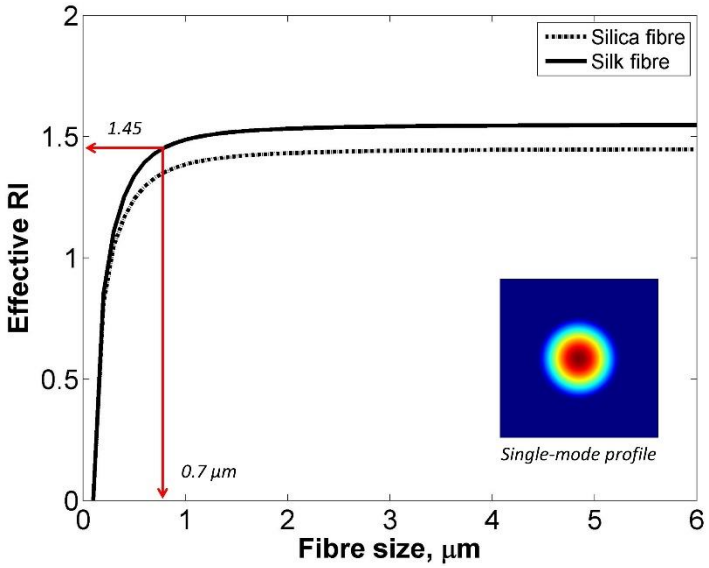

Figure 12: Effective index of fundamental mode for different of silica and silk fibre sizes.

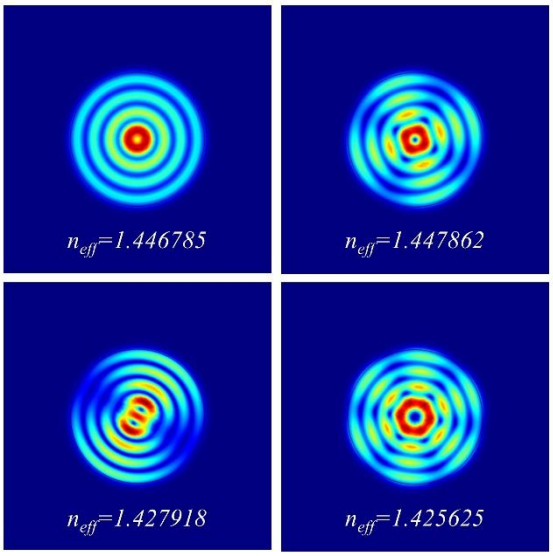

Figure 13: Electric field profile of some higher order modes in silk fibres.

In order to maximise the overlapping of electric field, the size of the injection fibre has to be scaled down to increase its evanescent field, shown in Figure 14. As the size of fibre decreases, the fraction of power in evanescent field increases. This can be done by tapering a standard silica optical fibre using a splicer. A Fujikura FSM-100P+ splicer was used to taper SMF-28 to the waist diameter of ~2-5 μm. It was then split into two half-tapers by breaking it in the middle. In practice, the tapered fibre was positioned sufficiently closed to the silk fibre using a micro-positioner; the tapered section would then be attracted and stuck to the silk fibre due to van der Waals force. The length of interaction was

judiciously adjusted using the longitudinal axis of the micro-positioner to optimise the coupling. Evanescent field coupling in visible wavelength was demonstrated, shown in Figure 15.

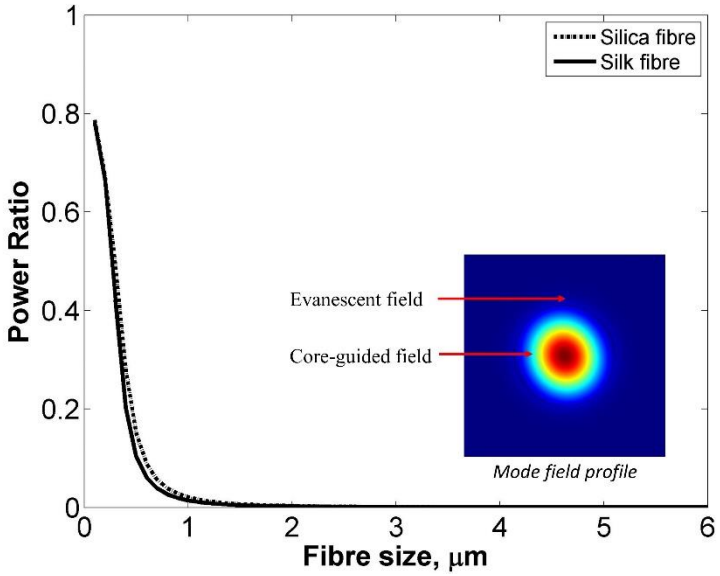

Figure 14: Power ratio of evanescent field over total power for different fibre sizes.

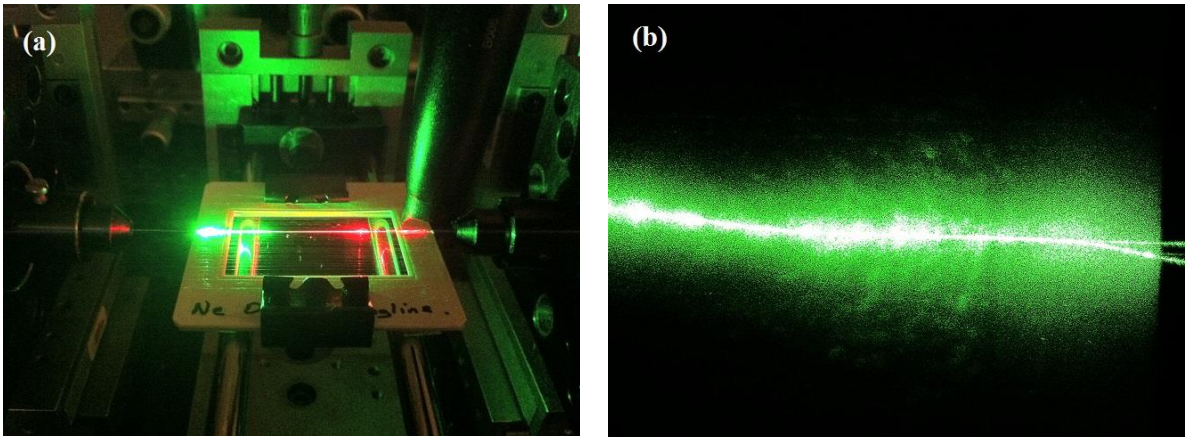

Figure 15: (a) Evanescent field coupling into the silk fibre sample from opposite directions using red and green lights. (b) Microscope view of the silk and tapered fibre co-propagating section.

4.2 Direct coupling

Direct coupling method has the advantage of wavelength independence but requires a smooth end facet to enable efficient light launching. In this project, we used two techniques to realise direct injection, which are through a bent section and a flat surface.

4.2.1 Direct injection from bent section

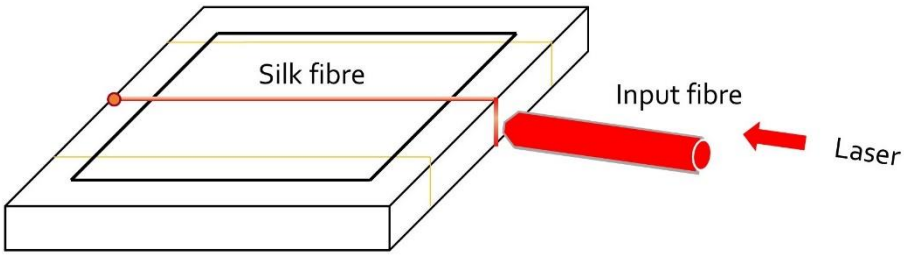

Figure 16: Experimental setup used for direct injection of light inside a bent silk fibre

A simple way to inject light directly into the silk fibre is through a bent section. A continuous stretch of silk fibre was wound on a plastic frame during fabrication. At the edge of the platform, the silk fibre formed a sharp bending of 180 degree with radius of ~0.5 mm as illustrated in Figure 16. The large RI difference between the silk fibre and the surrounding air resulted in a large light acceptance cone at the bent region; hence light can be coupled into the silk fibre with moderate precise alignment using a tapered lens fibre, as shown in Figure 17. Red light was scattered along the silk fibre and a red bright dot appeared at the other sharp bending of the same strand, indicating exiting point of light from the silk fibre, shown in Figure 18. Although light could be guided, this configuration has the problem of coupling out light as the output has a wide and irregular scattering angle.

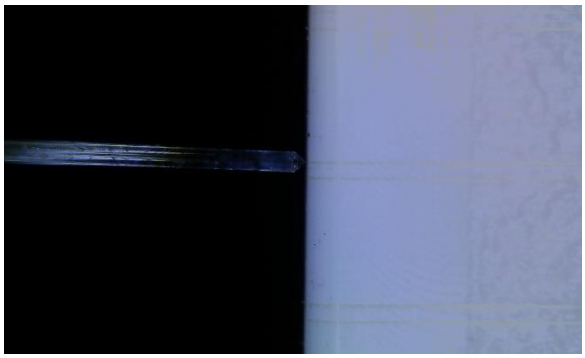

Figure 17: Precise alignment using tapered lens fibre for direct injection from bent section.

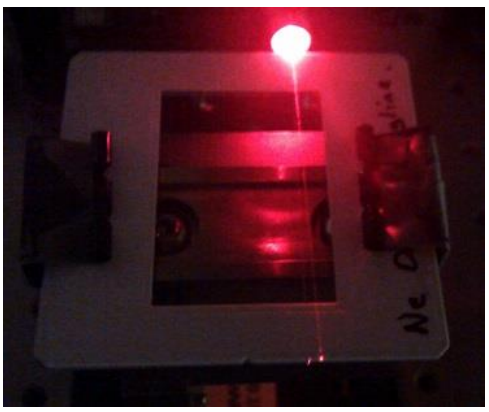

Figure 18: Image of light coupling by injecting light through a bent section. Red bright dot at the end indicates light exiting the silk fibre.

4.2.2 Direct injection into a flat surface

The other method is by direct injection through a fibre cross-sectional surface. The two end surfaces of the silk sample were properly cut and prepared. Light was launched into and coupled out from the silk fibre using SMF-28 fibre pigtails. Alignment was optimised with two micro-positioners monitored under microscope, shown in Figure 19.

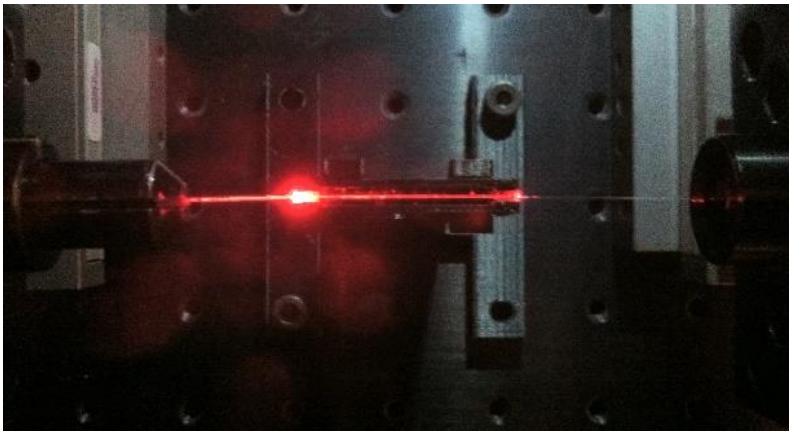

Figure 19: Direct injection into silk fibre through end surface.

The method had been tested on 5 samples, 3 of which are from the spool spun at 5 mm/s (core diameter of 5.6 μm) and another 2 are from the spool spun at 37 mm/s (core diameter of 5.0 μm). We have managed to inject light in all these samples; therefore validating the fact that light injection and guiding can be experimentally achieved in spider silk draglines.

5 OPTICAL CHARACTERISATION OF THE DRAGLINE SILK FIBRE

In this section, all the optical characterisation performed at EPFL-GFO on the dragline silk samples provided by Oxford Silk Group will be described. This is a very important task since it will give us precious information on some optical parameters of the silk fibre such as its propagation losses, birefringence and spectral features, allowing us to determine the best sensing technique(s) that can be employed for the detection of targeted biochemical agents.

5.1 Optical transmission window

First of all, a spectral characterisation of the dragline silk fibre was performed to determine its optical transmission window. Pre-alignments were performed with a red laser. Light from a supercontinuum source, used as broadband source, was then launched inside the silk fibre. An optical spectrum analyser (OSA) was used to collect the light transmitted through the silk fibre.

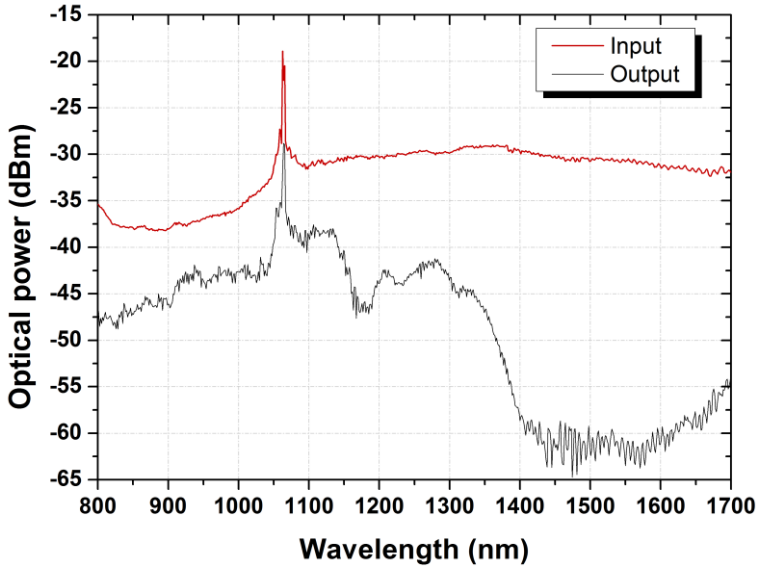

Figure 20: Measured optical spectrum at the input and output of a silk fibre sample.

The optical spectrum (800 nm – 1700 nm) measured at the input and output of the silk fibre is plotted on Figure 20. The difference between these two measurements gives the transmission losses with respect to wavelength, which were evaluated for two silk fibre samples of different core diameters (Figure 21).

This graph cannot be used to estimate the propagation losses with respect to wavelength inside the dragline silk fibre since the measured transmissions losses include coupling losses from both the injection and reception ends, which cannot be evaluated. Nor can it be used to compare the propagation losses with respect to the core diameter of the silk sample since the coupling losses for both samples are unlikely to be similar. However, comparison between the relative propagation losses with respect to wavelength for one sample can be made since the coupling losses are unlikely to vary by a big amount according to wavelength. Some pieces of information worth mentioning are:

- The transmission window in the silk dragline extends from 800 nm till 1350 nm. After this wavelength, the transmission losses drop by 20 dB (i.e. 100 times more).
- The wavelength range with less propagation losses is situated in the region of 900 – 1100 nm. It can potentially be a good working transmission window since optical components operating at this wavelength can be obtained (Nd:YAG emission wavelength is 1064 nm).

- The transmission losses (> 25 dB compared to the losses at 900 nm) in the typical bandwidth used in telecommunication (1500 - 1600 nm) is too high making it extremely difficult, if not impossible, to work in this region.
- **A good trade-off is to work in the 1300 nm (O-band) region.** The relative propagation losses in this region is < 10 dB compared to that at 900 nm and most optical components are available in the O-band region (formerly used as telecom window).

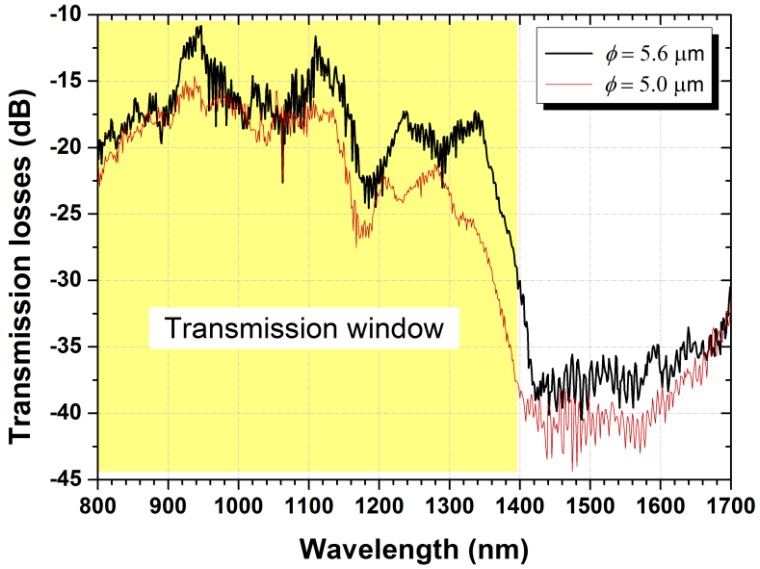

Figure 21: Transmission losses between 800 nm and 1700 nm for silk samples of two different core diameters.

5.2 Propagation losses

When light propagates as a guided wave in a fibre, it experiences some losses due to many factors such as intrinsic absorption by the material and Rayleigh scattering. In a fibre, the propagation losses are given in terms of an attenuation coefficient α, which represents the relative power lost per kilometre (dB/km) or per metre (dB/m) for very lossy fibres or waveguides.

Propagation loss is one of the most important parameters for an optical fibre. Measurement of propagation losses for a fibre is fundamental to optical system design, implementation, and performance estimation. In our case, this parameter will determine the length of fibre that can be used and hence the range and/or sensitivity of the sensor.

Table 5: Different techniques used to measure the propagation losses in a fibre. For the silk fibre, the most suitable method is the scattered light image analysis technique.

Method	Feasibility	Difficulty with silk fibre
Optical Time Domain Reflectometry	++	Long fibre sample needed
Waveguide-inspired non-destructive method	-	Applicable only for single-mode fibres (silk is multimode)
Cut-back measurement	++	Destructive method Difficult to cleave
Optical Frequency Domain Reflectometry [30]	--	Complicated setup
Scattered light image analysis technique	+	Scattering spots on spider dragline

Several techniques (Table 5) can be used to measure the attenuation coefficient α, which represents the relative power loss per metre (dB/m). For instance, a non-destructive technique [31], derived from a method used to measure the optical losses of waveguides, can be used. We have successfully managed

to use this technique to accurately measure the attenuation coefficient of small-core photonic crystal fibres in another research project. The basic assumption of this method lies in the fact that the linear losses are unchanged irrespective of the extremity of the fibre from which light is coming from. However, this is only true in the case of single-mode fibres rending this technique not suitable to measure the attenuation losses of the spider silk dragline.

Optical time domain reflectometry (OTDR) and the cut-back method [32] are most commonly used due to their simplicity and accuracy. However, for the OTDR, the fibre must be long enough (at least several metres), to allow the separation between the input pulse and the reflected signals; therefore making this technique not applicable for the silk dragline fibre.

The cut-back method, though simple to set-up and implement, is not suited as well for our silk sample because the silk fibre must always be kept strained for it to guide light properly thus prohibiting cleaving or breaking as in conventional silica-based optical fibre handling. This renders the use of cut-back method to estimate the attenuation coefficient α very challenging prompting the use of a non-invasive method, namely the scattered light image analysis technique, which is commonly used for determining optical losses in optical waveguides [33].

5.2.1 Experimental bench

The scattering loss-measurement technique involves the measurement of the propagated light scattered from the dragline silk fibre as a function of position. This light is taken to be proportional to the intensity in the fibre at that position, thereby assuming the scattering to be uniform throughout the fibre.

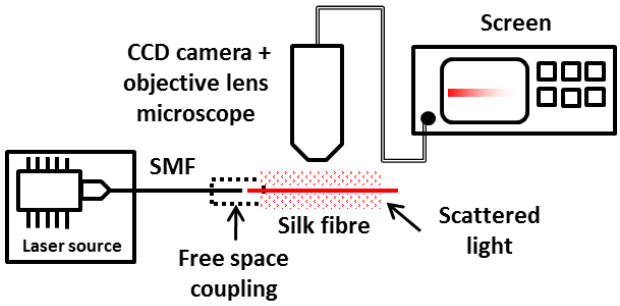

Figure 22: Experimental setup to measure the propagation losses along the dragline silk fibre using an image analysis technique.

The experimental bench used to measure the propagation losses along the silk fibre is shown on Figure 22. A top view detection system to observe the scattered light from the silk fibre was configured with a charge-coupled device (CCD) camera which is sensitive in both visible spectrum and near infrared region to capture the light streak scattered out from the fibre (for example Figure 23).

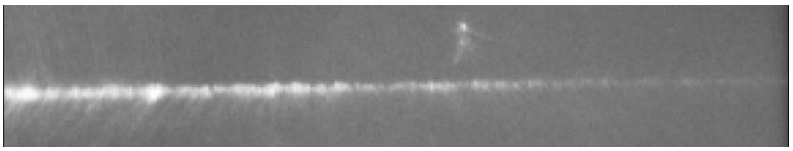

Figure 23: Micrograph captured with a CCD camera used for estimating the propagation loss of the silk sample from the distribution of scattered light intensity.

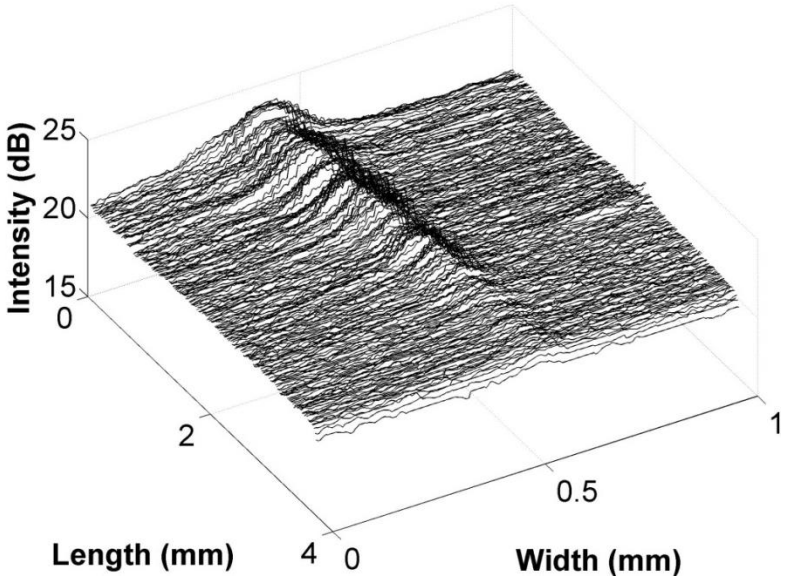

Figure 24: 2-D intensity profiles of the scattered light along the propagation direction of the light along the dragline silk.

Figure 24 shows the 2-D light intensity profile along the line streak directly derived from the output video signal. In order to obtain this graph, a background noise measurement (measurement without any light) was subtracted from the captured photo to compensate for any nonlinear sensitivity of the CCD camera or external light sources.

5.2.2 Results

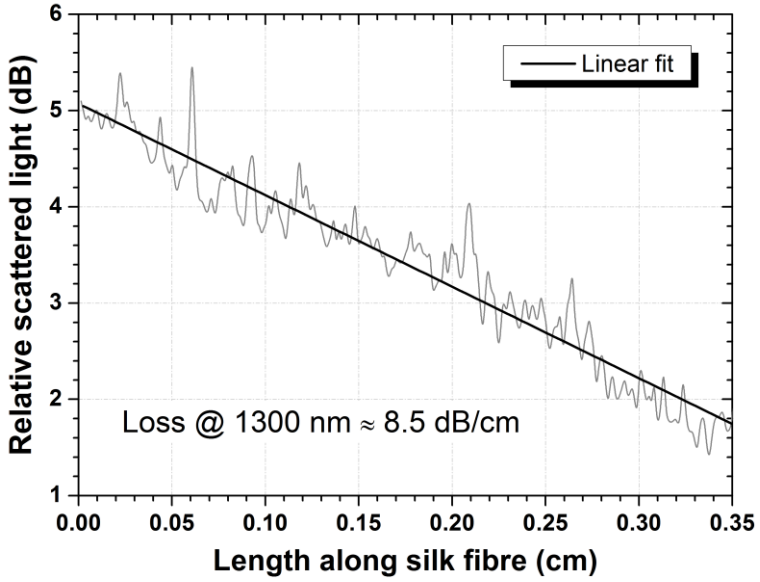

Figure 25: Relative scattered power as a function of the propagation length along the dragline silk fibre in the region of 1300 nm.

The longitudinal variation of the intensity of the scattered light along the silk fibre is obtained by taking the peak intensity variation across a section of the silk fibre along the propagation direction. Figure 25 represents the relative scattered power (in dB) as a function of the propagation length along

the dragline silk fibre in the region of 1300 nm. To obtain the corresponding propagation loss, the measured points are linearly fitted and the corresponding slope gives the value of α.

During some measurements, unexpectedly irregular high scattering points, due to defects in the fibre (dusts on silk fibre, presence of lipids etc.), were observed on some silk fibres. These points were not taken into consideration to avoid skewing the estimation of the value of propagation losses of the silk fibre.

Table 6: Measured values of α at different wavelengths

Wavelength(nm)	α (dB/cm)
650 nm	5±2
1302 nm	9±2
1550 nm	n/a

To obtain the best possible estimation of the propagation losses, a statistical approach involving the evaluation of the losses over seven 0.35 cm segments using two different fibres from the same dragline spool was adopted. Although being very time consuming, it was the only way to obtain reliable values due to all the uncertainties linked to this measurement. After averaging all the data, propagation loss is estimated as 5±2 dB/cm for red light and 9±2 dB/cm in the O-band region (Table 6). Several attempts to measure the losses in the C-band (1550 nm) proved to be unfruitful due to the anticipated very high propagation losses at this wavelength.

5.3 Birefringence

In an ideal, circular-core fibre made of an isotropic material such as glass, the two orthogonally polarised HE_x and HE_y modes supported by the fibre propagate with the same phase velocity. However, in reality, this is not the case since fibres are not perfectly circularly symmetric. This gives rise to a "fast" and a "slow" axis with different refractive indices of respectively n_y and n_x; the difference between these two values being called the modal birefringence B of the optical fibre:

$$B = n_y - n_x \qquad (2)$$

Typical silica SMF-28 fibres used for telecommunication purposes are very uniform and have therefore very low birefringence values of the order of 10^{-7}.

Table 7: Different methods commonly used to measure the birefringence between the two orthogonal polarisation modes in an optical fibre

Method	Limitation
Twist-test [34]	Difficult to apply for short fibres
Electro-optical or magneto-optical modulation [35]	
Cut-back [36]	Destructive method
Wavelength-scanning method [37]	--

Image-contrast immersion [38] could have been used to estimate the birefringence of the spider dragline silk fibre, but this method requires the knowledge of an approximated value for the RI of the dragline from the *Nephila edulis*, which we do not know, to find a suitable index-matching liquid. Since light injection can be achieved in these silk fibres, simpler techniques, listed in Table 7, used to measure birefringence in optical fibres can be employed.

5.3.1 Experimental setup

Instead, a simpler method based on a wavelength-scanning method [37] was used to evaluate the birefringence of the silk fibre in the O-band region (1302 nm).

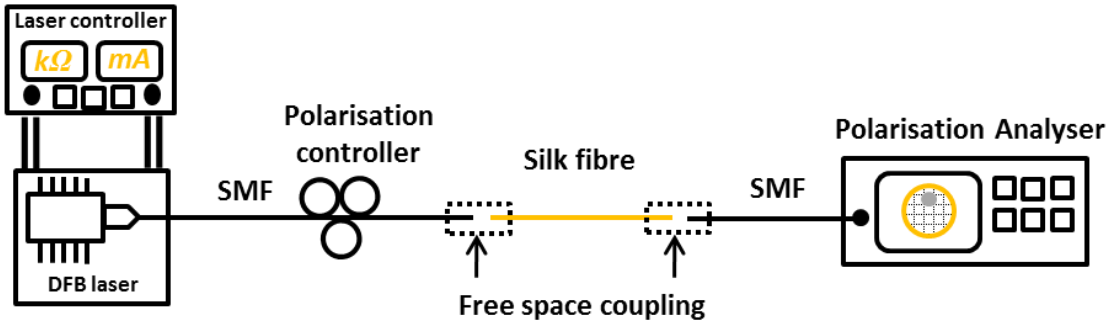

Figure 26: Experimental setup to measure the birefringence of the dragline silk fibre with the wavelength sweeping method.

The birefringence B of a fibre of length L is linked to the phase difference φ between the two orthogonally polarised modes at the output by the following equation:

$$\varphi = \frac{2\pi}{\lambda} B.L \qquad \textbf{(3)}$$

In our setup (Figure 26), a polarisation analyser was used at the output to measure the Stokes parameters linked to the state of polarisation (SOP) of the transmitted light, out of which φ was then evaluated. In our proposed method, the wavelength λ of the light source is swept by a small amount $\Delta\lambda$, where $|\Delta\lambda| << \lambda$. This wavelength change induces a change in φ such that:

$$\frac{\Delta\varphi}{\Delta\lambda} = \frac{-2\pi}{\lambda^2} B.L \qquad \textbf{(4)}$$

$$\Rightarrow B = -\frac{\Delta\varphi}{\Delta\lambda} . \frac{\lambda^2}{2\pi L} \qquad \textbf{(5)}$$

Light with a circular polarisation was injected into a silk fibre of length L=2.5 cm. A DFB semi-conductor single-mode laser, emitting at around 1302 nm, was used as a light source. By changing the laser's temperature, its wavelength was tuned over 1 nm and the corresponding φ phase difference induced by the dragline silk fibre was measured.

5.3.2 Results/conclusions

Figure 27 shows the wavelength dependence of φ for a silk fibre with a core diameter of 5.6 µm. The measured values were linearly fitted to obtain the slope of this graph (-3.92 rad/nm). By injecting this value into equation (5), a birefringence B of $\mathbf{4.23\times10^{-2}}$ was obtained for this sample.

The same procedure was applied to determine the birefringence of all the other silk fibre samples fabricated during this project. Typically, measured values of the birefringence ranged from $\mathbf{10^{-2} - 10^{-3}}$; which is at least an order of magnitude higher than that of conventional polarisation-maintaining fibres, e.g. PANDA fibres $B = 10^{-4}$. Hence, spider dragline silk can be considered as a highly birefringent fibre.

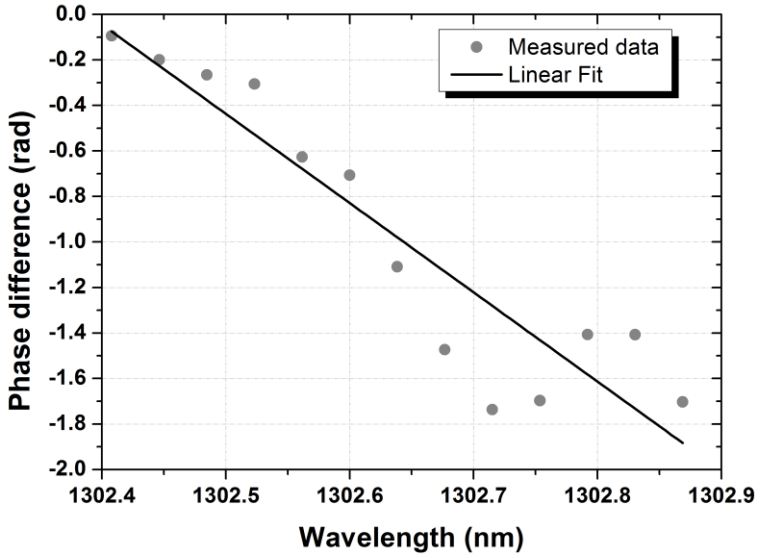

Figure 27: Phase difference φ between the two orthogonally polarised modes as a function of the wavelength.

It was difficult to link core diameter and fibre core diameter since fibre samples made from the same spool did not have similar measured values of birefringence. This can be explained by the presence of defects (presence of lipids etc.) or very small non-uniformity in the core diameter during the drawing process. Moreover, lower reeling speeds result in partly converted crystallinity and thus also in more amorphous fibres that will have much more variations.

6 DETECTION OF BIOCHEMICALS WITH THE SILK FIBRE

Optical fibre sensors that make use of the whole length optical fibre as the sensing element are usually used as distributed sensors. This means that each point along the fibre can separately and selectively sense quantities such as temperature, strain and pressure such that the fibre can distinctively inform on the position of the stimulus and on its magnitude. Distributed optical fibre sensors have today demonstrated their capability to measure quantities such as strain and temperature over tens of km with an excellent accuracy, essentially thanks to the extreme transparency of the glass fibres. Using the most advanced nonlinear interactions, up to 100,000 distinct sensing points can be resolved along a single optical fibre, meaning that a quantity can be selectively measured each metre over some 100 km, or each millimetre over 100m.

However, due to very large values of transmission losses (order of a few dB/cm), long lengths of silk fibres cannot be used, implying that distributed sensing cannot be considered as a viable option at this stage. Alternatively, the silk fibre can be used as an integrating sensor for the measurement of a particular measurand at a given position, in which the cumulated effect of the optical change in the fibre is integrated all over the fibre length to enhance sensitivity. The idea here is to use some target chemicals such as alcohols, ammonia, acetic acid, water, etc. Under the influence of the biochemical vapours, the dragline silk fibre will undergo a change in its material properties thereby inducing a change in the properties of light transmitted along the fibre. Several sensing techniques, inspired from currently employed methods, which can possibly be used for optical sensing of biochemicals, include:

- **Polarisation response and modified birefringence**: Polar molecules can modify hydrogen bonds within and between molecular chains, causing the latter to coil and uncoil. This effect will be translated into a change in the silk's birefringence, which can be detected by monitoring the state of polarisation (SOP) of the transmitted light using a polarisation state analyser.
- **Differential absorption spectroscopy**: In silk optical fibres, changes in optical transmission around fingerprint absorption features will be due to conformational changes induced by chemical compounds in the silk molecular structure. Several silk absorption features can be found around 1200-1500 cm^{-1} due to molecular vibrations of disordered α-helice and crystalline β-sheet domains. Silk transmission properties in the whole VIS-near IR wavelength region can be characterised using supercontinuum sources to identify potential silk overtone bands.
- **Fluorescence spectroscopy**: Tryptophan, an aromatic amino acid contained in silk proteins, exhibits strong intrinsic fluorescence that varies with the local microenvironment. An analysis of the excitation - emission matrix of the silk fibre could yield essential information about chemical species binding to protein macromolecules, as well as information regarding the silk structure such as the number of crystalline β-sheet domains contained in the silk fibre (level of crystallinity).
- **Raman spectroscopy**: The Raman silk spectrum is a signature of the molecular structure of the material and is particularly useful for studying conformational changes in proteins [39]. Raman spectroscopy offers many advantages: it can be performed at any wavelength and it shows sharp spectral peaks, increasing the sensitivity to changes in the molecular structure. It is interesting to note that the Raman shifts are of the same order of magnitude as that observed in silica fibres, corresponding to ~100 nm at near IR wavelengths [40], thus measurable using a high-resolution optical spectrum analyser operating in the C-band.
- **Microfibre knot resonators:** An alternative solution is to use the silk filament as a ring resonator. A sub-micron size silk sample is tied into a knot with a diameter of the order of a few hundred μm and light is brought inside and outside of this resonator through evanescent field coupling using tapered tips. Any change in the RI of the silk sample brought by the presence of a biochemical will shift the resonant transmission spectrum which can be easily measured in the optical domain.

Table 8: Different optical sensing techniques commonly used for biochemical detection

Method	Feasibility	Limitation
Polarisation response (induced birefringence)	+	
Differential absorption spectroscopy	-	No apparent presence of absorption peaks in the 600-1700 nm band
Fluorescence spectroscopy	-	Difficulty to collect all the fluorescent light from the silk
Raman spectroscopy	--	High power source needed
Microfibre knot resonators	--	Difficulty in making the knot resonator/light injection by evanescent field coupling

For obvious limitations listed in Table 8, only one of the listed sensing techniques can currently be considered in an attempt to demonstrate the proof-of-concept of biochemical detection based on spider silk dragline.

6.1 Principle

The birefringence of the silk fibre depends on both the overall degree of molecular orientation and the extent to which crystalline regions are present. Hydrogen bonds, within and between molecular protein chains, play a crucial role in the silk's structure. The presence of polar elements will gradually modify these bonds, causing the molecular chains to disorient and coil-uncoil [26]. This will change the overall molecular orientation inside the silk fibre and, therefore, induce a change ΔB in its birefringence.

This change in birefringence will induce a change in the phase difference $\Delta\varphi$ between the two orthogonally polarised modes according to the following equations:

$$\Delta\varphi = \frac{2\pi}{\lambda}\left(\Delta L.B + L.\Delta B\right) \quad \textbf{(6)}$$

$$\Delta L = 0 \Rightarrow \Delta\varphi = \frac{2\pi}{\lambda}.L.\Delta B \quad \textbf{(7)}$$

Note that a change in the length ΔL of the silk fibre (length L) can also induce a change in the phase difference $\Delta\varphi$. In our case, we can neglect this change since the fibre is placed under strain and tightly glued at both ends. By measuring this value of $\Delta\varphi$, the change in birefringence can easily be deduced using equation (7).

6.2 Experimental setup

The change in the phase difference between the two orthogonally polarised modes of light propagating along the silk fibre can be obtained by monitoring the SOP of the transmitted light using a polarisation state analyser.

The same experimental setup, described in the above section **5.3.1**, was used to detect several biochemical agents which impact the hydrogen bonding between the silk proteins within the silk fibre. Laser light at λ = 1302 nm was launched inside the silk fibre. The transmitted light was sent to a polarisation state analyser and set to a circular polarisation. A cotton bud soaked with the targeted biochemical agent was then placed close to but not in contact with the silk fibre to allow vapour-silk

interaction while simultaneously recording the SOP of the light guided through the silk fibre every 0.1 s for 15 s.

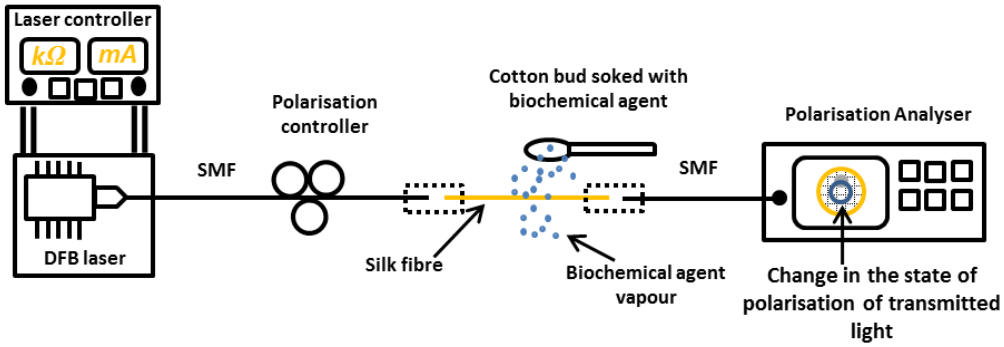

Figure 28: Experimental setup to measure the induced birefringence of the transmitted light along the dragline silk fibre brought by the presence of a biochemical agent.

The SOP of each time step was recorded as Stokes parameters (S_0, S_1, S_2, S_3). By taking the Mueller matrix for a rotated retarder, as described in [41], and setting the input Stokes as right or left circular polarised light, S_R=[1 0 0 1] or S_L=[1 0 0 -1], the phase change φ induced by the medium is simply equal to $\cos^{-1}(S_3)$ of the output Stokes. In the case of measuring the birefringence change, the initial output SOP is set to a circular polarisation and is assumed as the input SOP, thus the measured phase change is in reference to the initial SOP.

6.3 Results/conclusions

6.3.1 Small drift due to temperature fluctuations

First, a dry cotton bud (no biochemical) was placed next to the silk fibre. Figure 29(a) shows the change in the SOP of the transmitted light. One can notice a small shift in polarisation during this time even in the absence of biochemical agents. This small drift is brought by temperature fluctuations (person's presence, warm rising in measurement equipment, etc.). The change in phase difference corresponding to this drift is as low as 0.1 rad, as shown in Figure 29(b).

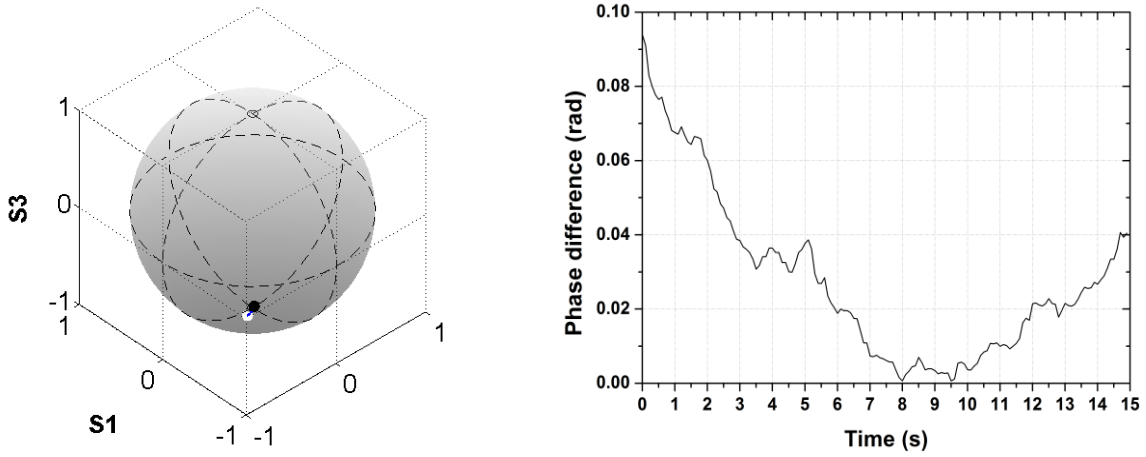

(a) **(b)**

Figure 29 : (a) Representation of the polarisation transformations on a Poincaré sphere of the transmitted light and (b) corresponding temporal change in phase difference $\Delta\varphi$. *White dot: initial state of polarisation; Black dot: final state of polarisation; blue line: path along sphere.*

6.3.2 Polar v/s non-polar biochemical agents

The same experiment was repeated with biochemical with different polarities.

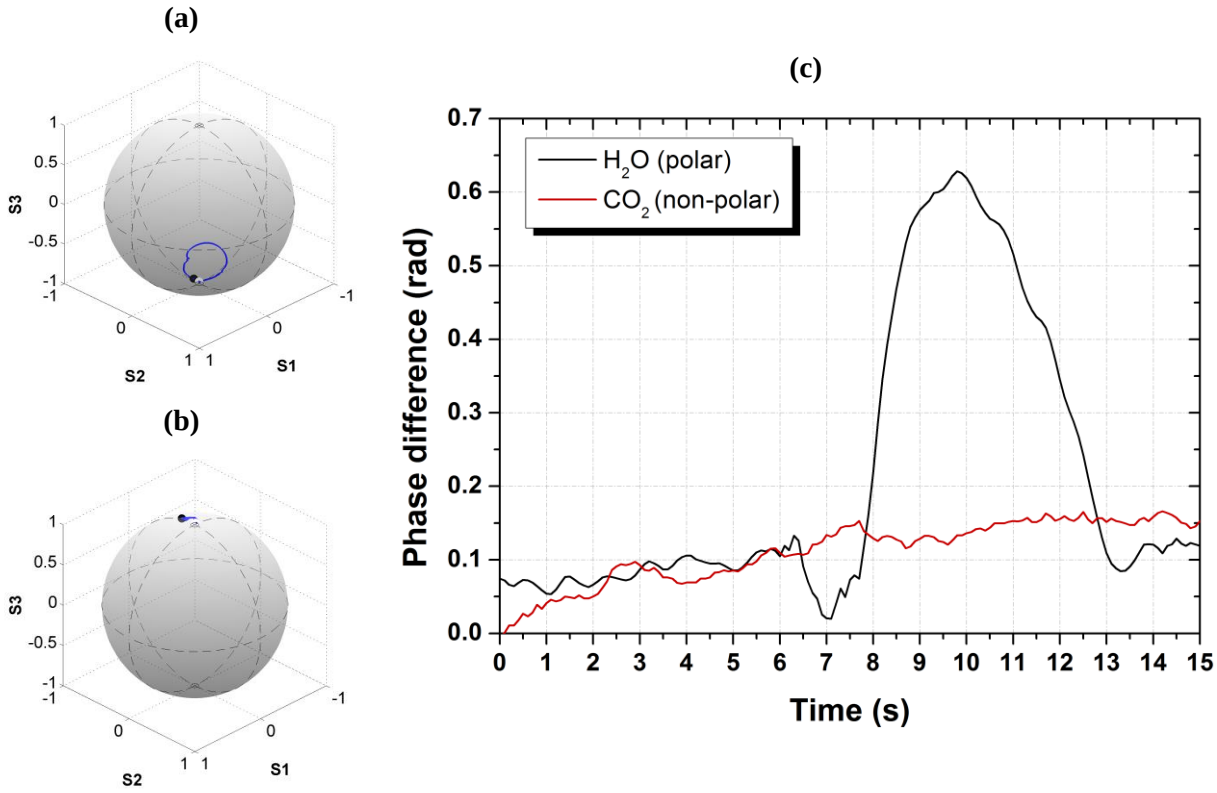

Figure 30 : Representation of the polarisation transformations on a Poincaré sphere of the transmitted light due to the presence of (a) water and (b) carbon dioxide vapours and (c) corresponding temporal changes in phase difference $\Delta\varphi$. *White dot: initial state of polarisation; Black dot: final state of polarisation; blue line: path along sphere.*

As soon as the cotton bud, soaked with water, was placed next to the silk fibre the SOP of the transmitted light instantaneously changed (Figure 30(a)) indicating a change in the fibre's birefringence. The temporal evolution of φ for this experiment is on Figure 30(c). Initially, the value of φ was constant since the silk fibre was left unperturbed. After 6 seconds, the cotton bud was placed next to the silk fibre. φ immediately changed with a response time of the order of the second and went back at to its initial phase when the cotton bud was removed.

On the other hand, the presence of non-polar molecules did not seem to impact on the birefringence of the silk fibre. When exposed to pure carbon dioxide gas, the silk fibre's birefringence did not change. Only a small drift, probably due to temperature, in the SOP of the transmitted light was observed (Figure 30(b)).

Two other hydrogen bond-active agents, namely acetic acid and ammonia, were tested and the corresponding Poincaré representations showing the change in SOP in each case is shown in Figure 31. Based on these figures, it is clear that the chemical agents induced a change in birefringence in the silk fibre.

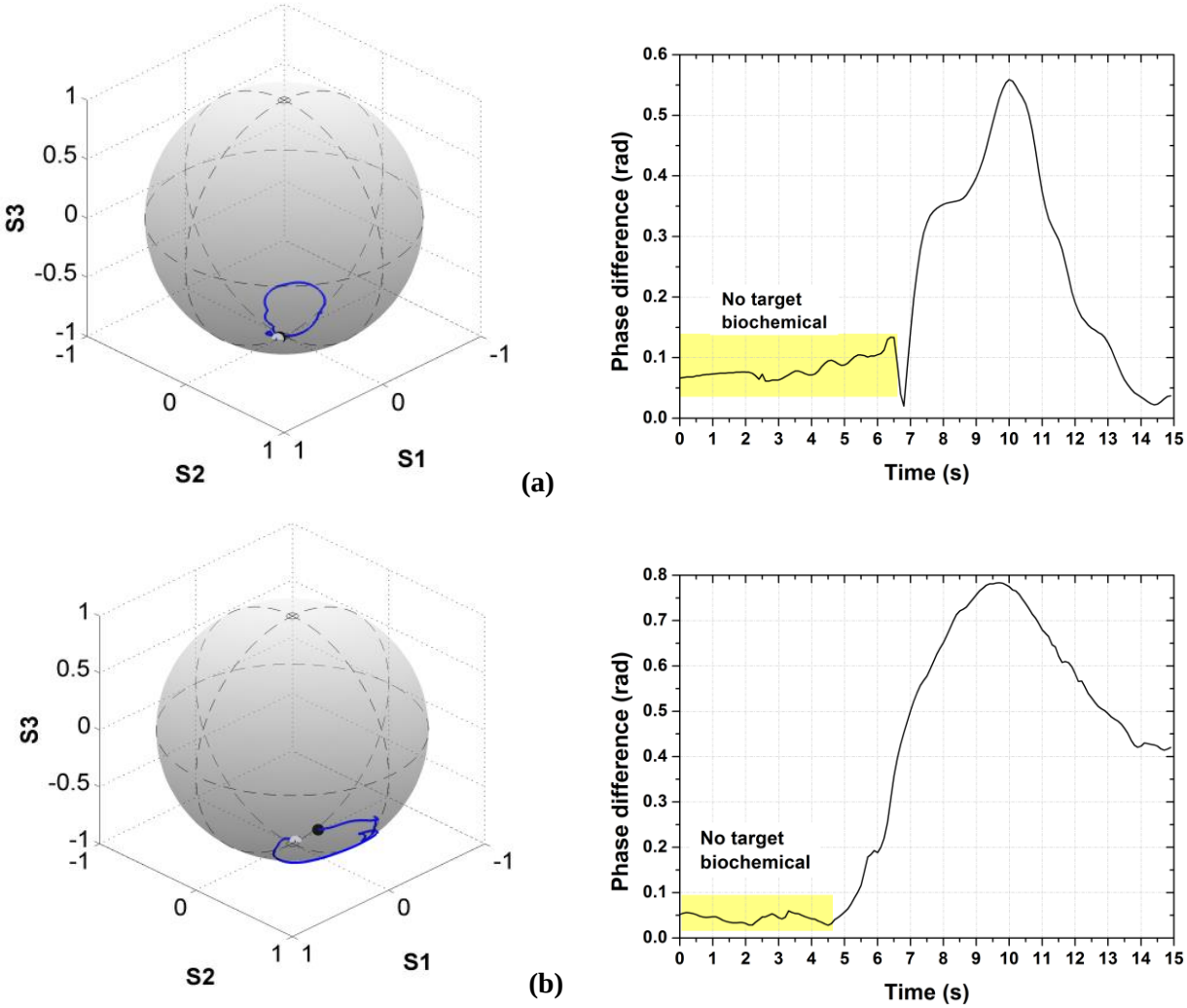

Figure 31 : **(Left)** Representation of the polarisation transformations on a Poincaré sphere of the transmitted light and **(Right)** corresponding temporal change in phase difference $\Delta\varphi$ brought by the presence of (a) acetic acid and (b) ammonia vapours. *White dot: initial state of polarisation; Black dot: final state of polarisation; blue line: path along sphere.*

Table 9: Change in birefringence induced by each biochemical compound.

Modifying agent	ΔB	Percentage change (%)
Water	5.11E-5	0.121
Acetic acid	4.59E-5	0.109
Ammonia	6.38E-5	0.151

The change in birefringence ΔB induced by each biochemical compound was determined and listed in Table 9. The 5 silk fibre samples fabricated during this project were tested with different biochemical agents (ammonia, water and acetic acid). All the samples reacted positively to the presence of these 3 target agents. Hence, the proof-of-concept of fibre bulk sensing using spider silk for biodetection of polar solvents has been demonstrated.

7 SPACE-RELATED ISSUES

7.1 Potential application of the sensor for space missions

Life on Earth depends on chemicals build-up from carbon and nitrogen. When these molecules break down they release gases like methane (CH_4) and ammonia (NH_3). Methanogenic bacteria are prime candidates for life on Mars, as they don't need oxygen or sunlight to survive but get their energy from CO_2 and hydrogen to make methane and water. Therefore looking for trace amounts of methane and water vapor is one attractive avenue to look for life on Mars. In the past, Earth-based telescopes operating at optical wavelengths and Mars-orbiting satellites such as ESA's Mars Express have been used to remotely detect e.g. methane gas on the red planet, both employing optical measurement techniques. Moreover *in-situ* detection of methane gas has been achieved at higher concentration using the Tunable Laser Spectrometer (TLS) instrument onboard Curiosity with a dedicated second channel operating at λ=3.27 µm for methane detection specifically [42]. The local detection of methane plumes at high concentration implies the production of methane on the red planet as its decay time is ~300 years, either via methanogenic bacteria or by geothermal activity, the mechanism for methane production being still unknown until now. Liquid water has also been detected in the Gale crater by the Curiosity rover, however without necessarily implying living organisms due to the low quantities detected [43]. Instead the presence of liquid water is thought to be due to Martian salts lowering the melting point of water.

Ammonia is another indicator of life but its detection has not yet been reported by neither the Mars Express nor by any other team. The Planetary Fourier Spectrometer (PFS) instrument onboard Mars Express analyses optical absorption lines to obtain e.g. temperature information but it does not have the resolving power to distinguish ammonia from carbon dioxide. Ammonia has a very small decay time ~1 hour after production, with its most likely source being the breakdown of proteins. Therefore finding ammonia would unambiguously indicate life on Mars.

In this study, we already showed that our sensor is very sensitive to water and ammonia vapours. The silk fibre is likely to be much more sensitive to water vapour than current detection methods used on Mars. Moreover, at the moment, no dedicated instrument is present for detecting ammonia in trace amounts. In the experiment below we address whether our sensor would be able to sense ammonia and water vapour in a Martian atmosphere. Detecting both of these gases would indicate life.

7.2 Detection of water and ammonia vapour over a CO_2 flow

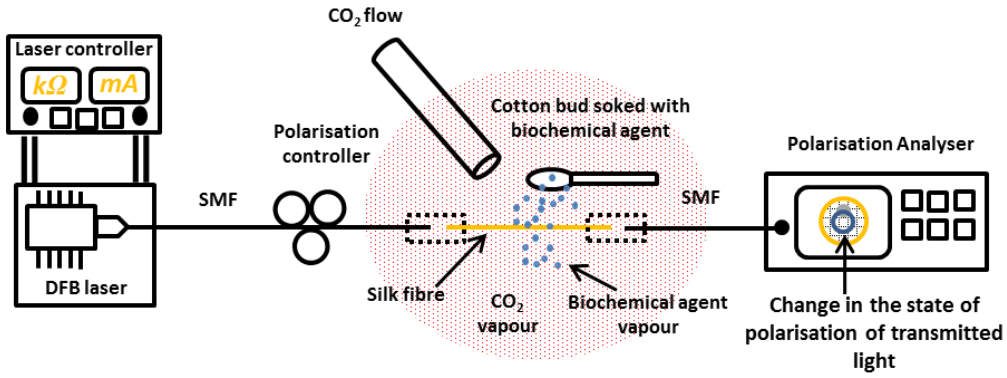

Figure 32: Experimental setup to detect the presence of ammonia and water vapours over a flow of CO_2.

The same experimental setup, described in the above section 6.2, was used to test whether the silk fibre would be able to sense ammonia or water vapour over a flow of carbon dioxide (akin to the Martian surface, with CO_2 gas being the prime atmospheric constituent at 6mbars). As shown in Figure 32, a constant flow of pure CO_2 gas was first released over the silk fibre and the temporal response of φ monitored over 55 seconds (Figure 33). During the first 10 seconds, a small shift of around 0.15 rad was observed before stabilising around this value. This small drift can be explained by the cooling effect brought by the flow of CO_2, which decreased the temperature of the silk fibre.

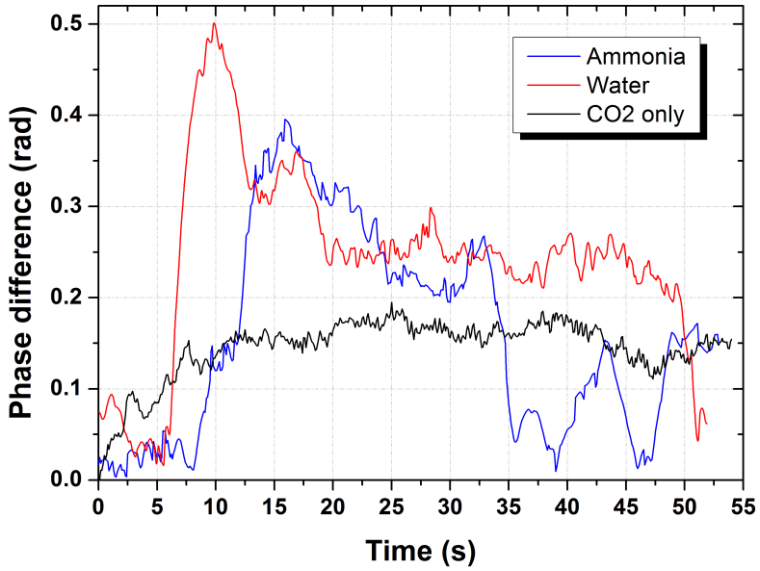

Figure 33: Change in $\Delta\varphi$ when ammonia and water is brought next to the spider silk sample.

As soon as the silk fibre was exposed with the polar biochemical agents, both induced a change in birefringence in the silk fibre (Figure 33). Despite the presence of a non-polar gas, CO_2, the silk fibre based FOB could still clearly detect the presence of ammonia and water vapours, indicating that our fibre sensing system could work in a Martian atmosphere. Since methane is also a non-polar molecule, we have strong reasons to believe that our ammonia and water detection system would not be affected by methane plumes on Mars.

8 CONCLUSION AND PERSPECTIVES

This report details the work performed during the Ariadna Study: "The Silky Way: Biomimetic Sensing Through Changes In Structural Proteins" performed by a collaborative consortium composed of Group for Fibre Optics (GFO) from Ecole Polytechnique Fédérale de Lausanne (EPFL) and the Oxford Silk Group from Oxford University in close partnership with the Advanced Concepts Team from the European Space Agency.

The potential of dragline silk as a new type of fibre optic biosensor has been explored in Silky Way. Sensing depends on the intrinsic material change rather than the small interaction region through evanescent field or small change in length through fibre tip found in most of the conventional optical fibre based biosensors. Silica optical fibres are commonly used for sensing physical parameters such as temperature, mechanical strain, vibrations, pressure acceleration, rotations (gyroscopes) but they are very poorly or even not at all sensitive to chemical or biological compounds. In the case of silk fibres, the elemental building blocks of dragline silk are proteins. Hence, the presence of some biochemical agents will directly modify the properties of the fibre material in its entire volume; thereby changing the properties of light propagating inside the fibre.

In developing spider silk based biosensor, we have demonstrated light guidance through silk fibre with two methods, evanescent field coupling and direct injection. Dragline silk can guide light as its RI (n~1.55) is higher than the surrounding (air). Evanescent field coupling method is non-invasive, which allows us to study the light guiding without cutting the dragline silk sample. Half-tapered fibre with tip diameter of ~4µm was fabricated and successfully used to launch visible light into the dragline silk sample. However, evanescent field coupling method is not suitable for spectral characterisation as the operating bandwidth is limited and the transmitted power is wavelength dependent. For these reasons, direct injection of light through a flat end facet of the silk fibre was preferentially used for more efficiency. This allowed optical characterisation of the silk fibre samples in terms of propagation losses (order of some dB/cm) and birefringence ($10^{-2} – 10^{-3}$).

Sensing of several chemical compounds has been demonstrated by recording the change in polarisation state of output light. The observation of fast response and high sensitivity of silk fibre towards polar chemical compounds (water, ammonia etc.) has shown promising application in biochemical vapour sensing. Polar molecules can modify hydrogen bonds within and between molecular chains, causing the latter to coil and uncoil. This effect will be translated into a change in the silk's birefringence, which can be detected by monitoring the state of polarisation of the transmitted light using a polarisation state analyser.

This sensor can potentially be used to detect the presence of water and ammonia traces in a Martian atmosphere since it is not sensitive to non-polar compounds such as carbon dioxide and methane, which mainly compose the Martian atmosphere.

The positive results obtained in the framework of Silky Way can potentially bring a major breakthrough in the optical fibre biosensing field. Firstly, the use of a sensing fibre made from a chemically sensitized material such as silk will considerably simplify the interrogation and detection sensing system since we will no longer require complex setups based on evanescent-field sensing. Secondly, this will pave the way for the fabrication of a new generation of economical and custom-made FOBs since spider silk can be spun at ambient conditions. Moreover, silks can be functionalized to be even more sensitive to any type of biochemical or particular environmental quantities by incorporating specific dyes making them very cost-effective for potential artificial industrial production of silk-based fibres with unique properties.

ACKNOWLEDGEMENTS

EPFL-GFO would like to thank the PHOTONIC SYSTEMS LABORATORY (PHOSL) and the NANOPHOTONICS AND METROLOGY LABORATORY (NAM) from EPFL for their kind support by providing equipment that were used in Silky way for the optical characterisation of the spider silk dragline.